Circulation

ORIGINAL RESEARCH ARTICLE

Single-Cell Sequencing of Mouse Heart Immune Infiltrate in Pressure Overload–Driven Heart Failure Reveals Extent of Immune Activation

Elisa Martini, PhD*
Paolo Kunderfranco, PhD*
et al

BACKGROUND: Inflammation is a key component of cardiac disease, with macrophages and T lymphocytes mediating essential roles in the progression to heart failure. Nonetheless, little insight exists on other immune subsets involved in the cardiotoxic response.

METHODS: Here, we used single-cell RNA sequencing to map the cardiac immune composition in the standard murine nonischemic, pressure-overload heart failure model. By focusing our analysis on CD45$^+$ cells, we obtained a higher resolution identification of the immune cell subsets in the heart, at early and late stages of disease and in controls. We then integrated our findings using multiparameter flow cytometry, immunohistochemistry, and tissue clarification immunofluorescence in mouse and human.

RESULTS: We found that most major immune cell subpopulations, including macrophages, B cells, T cells and regulatory T cells, dendritic cells, Natural Killer cells, neutrophils, and mast cells are present in both healthy and diseased hearts. Most cell subsets are found within the myocardium, whereas mast cells are found also in the epicardium. Upon induction of pressure overload, immune activation occurs across the entire range of immune cell types. Activation led to upregulation of key subset-specific molecules, such as oncostatin M in proinflammatory macrophages and PD-1 in regulatory T cells, that may help explain clinical findings such as the refractivity of patients with heart failure to anti–tumor necrosis factor therapy and cardiac toxicity during anti–PD-1 cancer immunotherapy, respectively.

CONCLUSIONS: Despite the absence of infectious agents or an autoimmune trigger, induction of disease leads to immune activation that involves far more cell types than previously thought, including neutrophils, B cells, Natural Killer cells, and mast cells. This opens up the field of cardioimmunology to further investigation by using toolkits that have already been developed to study the aforementioned immune subsets. The subset-specific molecules that mediate their activation may thus become useful targets for the diagnostics or therapy of heart failure.

*Drs Martini and Kunderfranco contributed equally.

The full author list is available on page 2105

Key Words: cardiac failure ■ cardiac toxicity ■ congestive heart failure ■ oncostatin M ■ programmed cell death, type I ■ sequence analysis, RNA

Sources of Funding, see page 2105

© 2019 American Heart Association, Inc.

https://www.ahajournals.org/journal/circ

Downloaded from http://ahajournals.org by on July 24, 2023

Clinical Perspective

What Is New?

- Single-cell sequencing allows precise identification of inflammatory/immune cell subpopulations in the diseased myocardium and may help find new targets for therapy.
- Proinflammatory cytokine oncostatin M, shown to mediate refractivity to anti–tumor necrosis factor treatments, is selectively expressed by the 2 most inflammatory subpopulations of macrophages recruited to the diseased myocardium, and was found in diseased but not healthy human myocardium.
- Cardiac regulatory T cells, an immunosuppressive population, selectively express PD-1, known to contribute to their anti-inflammatory function.
- In vivo treatment with anti–PD-1, used in immunotherapy regimes, unleashed cardiac inflammation and induced systolic dysfunction, offering a novel explanation for cardiotoxicity in tumor immunotherapy.

What Are the Clinical Implications?

- Single-cell sequencing of the inflammatory/immune cells in the hearts of mice, at different stages of a model of heart failure, provided insight into the complexity, dynamics, and extensive range of cellular networks regulating the immune response in the diseased myocardium.
- The immune response in the diseased myocardium features all the components of classical human immune responses, as with response to infection or autoimmunity, rendering existing knowledge on cytokines and immune cell populations of potential relevance to myocardial diseases.
- Oncostatin M and PD-1 emerge as components of the inflammatory/immune response in human heart failure and may be promising potential therapeutic targets.

Heart failure (HF) is characterized by inflammation. Stressing the myocardium triggers the release of proinflammatory cytokines.[1] The resultant immune response involves heart-infiltrating macrophages[2] required for disease progression.[3] T cells are also essential for the progression of pressure overload–induced HF.[4–6] On the basis of these findings, attempts are being made to modify immune responses to treat cardiovascular disease.[6,7] Yet, we know very little about the nature of immune cell activity in the ailing heart.

Single-cell RNA sequencing (scRNA-seq) has been applied to examine the noncardiomyocyte cell populations of healthy mouse[8,9] and post–myocardial infarction hearts.[10] Yet, the abundance of nonimmune infiltrating cells (eg, fibroblasts, endothelial cells) dilutes the less abundant—but potentially important—immune cell subpopulations, often beyond the threshold of detection. To address this shortfall, we used the pressure-overload transverse aortic constriction (TAC) model, where ligation of the aorta leads to hypertrophy, followed by dilated cardiomyopathy and HF with reduced ejection fraction.[11,12] We exclusively examined the infiltration of immune cells (CD45$^+$) in control hearts or hearts at the early or late stage of disease by using scRNA-seq.

We identified that the heart is populated not only by resident and infiltrating macrophages, CD8$^+$ and CD4$^+$ T cells, but also by infiltrating B cells, Natural Killer (NK) cells, dendritic cells, mast cells, and, less expectedly, neutrophils and regulatory T cells (Tregs). These findings were validated by multiparameter flow cytometry, immunohistochemistry, immunofluorescence staining of clarified cardiac tissue, and human patient biopsies. Cells from almost all of these subsets underwent extensive activation or expansion in response to disease. Thus, even though the trigger is hemodynamic stress, and not pathogen infection or autoimmunity, HF is characterized by a classical immune response, involving not only macrophages and T cells, but indeed most immune cell subsets. Because the tools for the study and manipulation of these subsets, and of the molecules that we show here are upregulated on activation, already exist for use in immunological diseases, the resource we have generated may enable identification of novel biomarkers and therapy targets for HF.

METHODS

Additional details are available in the Expanded Methods in the online-only Data Supplement, including Tables I through IV in the online-only Data Supplement and Figures I through XI in the online-only Data Supplement. Data, methods, and materials will be made available by the authors for the purpose of reproduction or replication.

Animals

All procedures were performed in compliance with national and European Union legislation, and Humanitas Research Hospital regulations.

Human Biopsies

Human biopsies were collected after informed consent according to the study protocols approved by the institutional review board of the Humanitas Research Hospital.

Statistical Analysis

All data sets were tested for normal distribution. For normally distributed data sets, unpaired *t* test, one-way ANOVA with Tukey post test, 2-way ANOVA with Tukey multiple comparison post test, and 2-way ANOVA with repeated measures and Bonferroni post test or paired *t* test were used, as most appropriate. The Mann–Whitney test was used to test statistical significance in data sets without normal distribution.

Downloaded from http://ahajournals.org by on July 24, 2023

Independent Data Access

The scRNA-seq data have been deposited in GEO (Gene Expression Omnibus) under accession code GEO: GSE122930.

RESULTS

Experimental Setup

To examine the immune cells present in the heart during HF, we operated on C57BL/6J mice, inserting a TAC via surgical suture thread ligation or performing a sham operation, where the thread was passed by the aorta but immediately removed. TAC operation led to a significant decrease of cardiac functionality in comparison with sham (Figure IA in the online-only Data Supplement). Mice were euthanized at 1 or 4 weeks after the operation, representing early versus advanced stages of disease. After tissue harvesting, CD45$^+$ cells were purified by flow cytometry (Figure IB in the online-only Data Supplement) and used for scRNA-seq. An outline of the procedures is shown in Figure 1A. We focused on CD45$^+$ cells, enabling higher resolution analysis of the immune subpopulations infiltrating the heart, used a rapid isolation protocol enabling the detection of populations such as neutrophils, which may not survive with lengthy purification protocols, and used biological duplicates to enhance robustness. Tissue-infiltrating cells may be harvested together with cells present in small capillaries. Prestaining with fluorescently labeled anti-CD45 immediately before the mice are euthanized and the vascular circulating cells are extracted, as in Bansal et al,[13] enables the distinction of true tissue-infiltrating from capillary-infiltrating immune cells, because only the latter are stained in vivo. Performing this control, both the standard perfusion-based protocol and our protocol yielded equal but high levels (≈50%) of capillary-infiltrating cells within the cells harvested from the tissue (Figure IIA in the online-only Data Supplement). Thus, heart-associated populations correspond to both true tissue-infiltrating immune cells and cells in small capillaries. This would be confounding for mapping any other tissue; yet immune cells are mobile, regulated by changes in activation state, which dynamically determines localization. Mapping the immune infiltrate is thus mapping of immune activation state. We found that immune cells present in capillaries were more similar to those found within the tissue, rather than those in the vasculature, suggesting that immune cells are found either in the tissue and its capillaries, or in transit to and from lymphoid organs (see the Validation section).

Heart Associated With a Wide Range of Immune Cell Subsets, Undergoing Drastic Changes Associated With Disease

The mRNA transcripts of the extracted tissue-associated single cells were analyzed using the 10X Genomics platform. Output was quality controlled (Table I in the online-only Data Supplement) and analyzed using the Seurat clustering algorithm.[14] The significant reproducibility (R>0.9, P <0.01) between biological replicates was confirmed (Figure IIB in the online-only Data Supplement). We applied unsupervised Seurat clustering on the pool of all samples analyzed (see Expanded Methods in the online-only Data Supplement), to maximize detection resolution. The resolution tree of the clusters, including an additional subcluster layer, is shown (Figure IIC in the online-only Data Supplement). We identified 20 clusters of CD45$^+$ cells (Figure 1B and Figure IID in the online-only Data Supplement). The clusters were represented in all 4 conditions, 1 and 4 weeks after TAC; 1 and 4 weeks after sham (Figure 1C, and Figure IID in the online-only Data Supplement). The immune subsets in each cluster were readily identifiable based on significant expression of well-characterized marker genes (Figure 1D, and Figure III in the online-only Data Supplement). Pearson correlation analysis (Figure 1E) revealed groups of clusters with similar transcriptional profiles, coinciding with the main immune cell type identities. The most abundant cell populations were macrophages/monocytes (clusters 3, 4, 5, and 8) and B cells (clusters 0, 2, 11, and 17), followed by NK cells (clusters 1 and 12). CD8$^+$ T cells appeared in 2 distinct clusters (clusters 6 and 15), as did CD4$^+$ T cells (clusters 9 and 13). For the first time in a heart scRNA-seq study, we identified the presence of 2 clusters of neutrophils (clusters 7 and 16). Cluster 10 corresponded to dendritic cells, whereas cluster 14 corresponded to Tregs. Mast cells, implicated in the past in cardiac disease,[15,16] also appeared in cluster 19. The cluster numbers correspond to the relative abundance of each cluster within the pooled samples. Ordering these clusters according to abundance, in each condition separately, uncovers the surprising finding that at the late stage of disease (4 weeks after TAC), a major reshuffling in cluster order occurs (Figure 1F, Tables II and III in the online-only Data Supplement). This can be attributed only to activation-induced expansion of different immune subsets in response to cardiac stress. In other words, the cardiotoxic immune response clearly involves several immune cell subsets that collectively mount what macroscopically is seen as cardiac inflammation.

Downloaded from http://ahajournals.org by on July 24, 2023

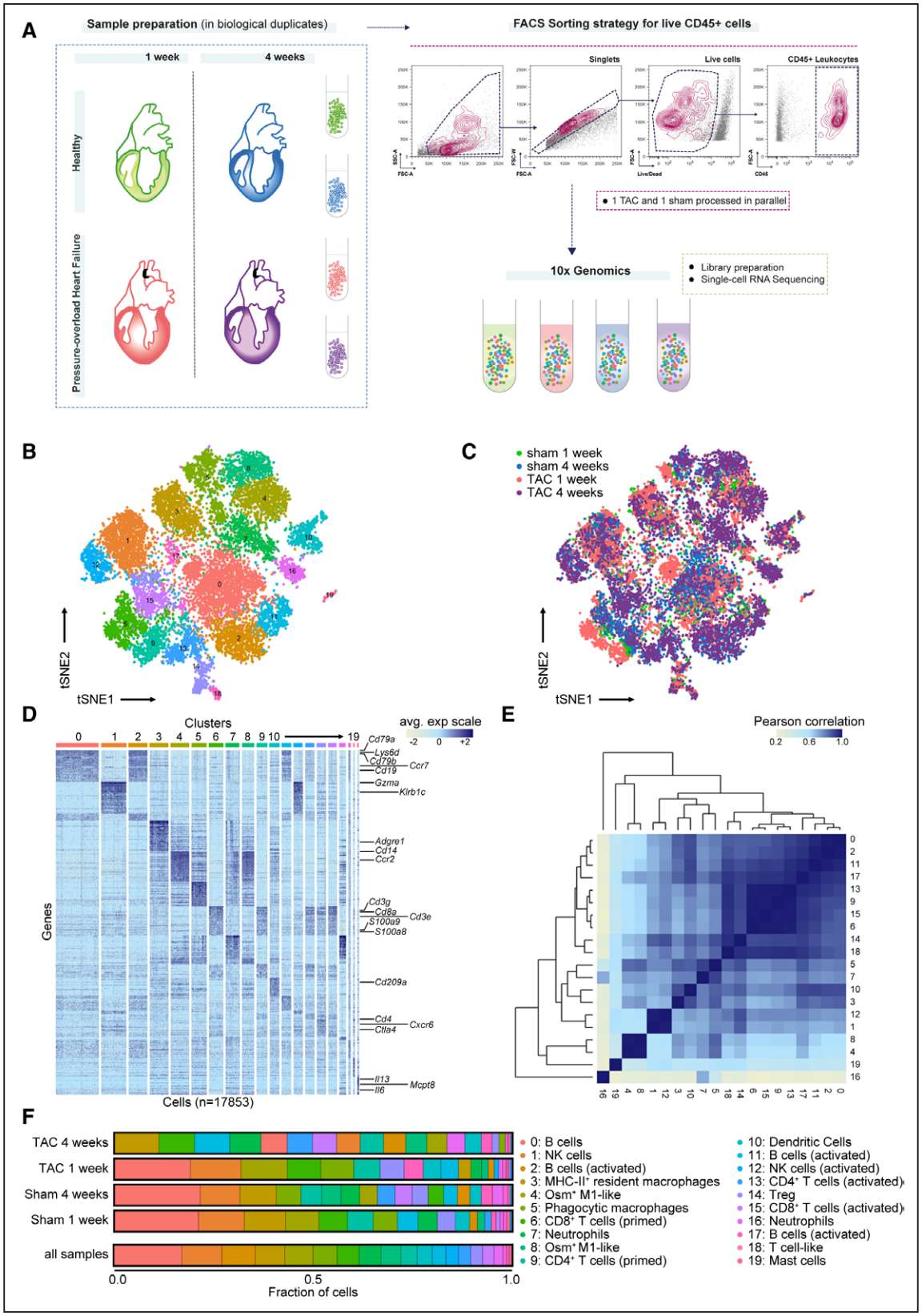

Figure 1. Single-cell RNA sequencing of cardiac CD45⁺ cells reveals the presence of 20 immune cell clusters.
A, Graphical representation of the experimental setup. Samples were isolated from hearts of TAC- or sham-operated C57BL6/J male mice 1 or 4 weeks after surgery, in duplicates. One TAC- and 1 sham-operated mouse for each time point were processed in parallel. Hearts were digested and live CD45⁺ cells were FACS-sorted and loaded for scRNA-seq. **B**, Two-dimensional *t*-distributed stochastic neighbor embedding (t-SNE) visualization of 17 853 cardiac CD45⁺ (immune) cells identified 20 different clusters after unsupervised clustering. Each point depicts a single cell, colored according to cluster designation. **C**, t-SNE projection of all cardiac immune cell populations (as in **B**) colored by experimental condition (green: sham at 1 week, blue: sham at 4 weeks, red: (*Continued*)

Downloaded from http://ahajournals.org by on July 24, 2023

Resident and Recruited Macrophage/Monocyte Populations

Macrophages were one of the most abundant immune cell types in the heart. We identified 4 distinct clusters significantly expressing macrophage/monocyte markers: clusters 3, 4, 5, and 8 (Figure 1D, Figure III in the online-only Data Supplement, Figure 2A, and Figure IVA in the online-only Data Supplement). Cardiac macrophages are classified as CCR2⁻ resident macrophages and CCR2⁺ recruited proinflammatory monocyte/macrophages.[2,3,17,18] Analyzed against gene signatures for CCR2⁺ versus CCR2⁻ cardiac macrophages,[17] only cluster 3 had a significant association with CCR2⁻ macrophages, whereas clusters 4, 5, and 8 correlated with the signature for CCR2⁺ proinflammatory macrophages (Figure 2B). Yet, cluster 5 did not express high levels of *Ccr2* mRNA, and the highest mRNA signals for *Ccr2* among all clusters were indeed found in clusters 4 and 8 but not 5 (Figure 2C), suggesting that cluster 5 was CCR2⁻, yet transcriptionally distinct from cluster 3. Recent work has identified 2 distinct CCR2⁻ populations[18]; we thus tried to better distinguish the 2 CCR2⁻ populations, 3 and 5.

Cluster 3 significantly expressed M2-like markers *Cd163* and *Mrc1*, high levels of major histocompatibility complex (MHC) II molecules, and was significantly correlated with antigen processing and presentation (Figure 2D, Figure IVB in the online-only Data Supplement, and Figure 2E); thus, cluster 3 may correspond to pro-repair, MHC II^{hi} cardiac tissue–resident macrophages thought to fulfill an immunosurveillance function.[2] Cluster 5 lacked CCR2 expression, had low expression of MHC II molecules, and was significantly correlated with phagocytosis (Figure 2B and 2C, Figure IVB in the online-only Data Supplement, and Figure 2F); thus, cluster 5 could be the cardiac-resident population contributing to homeostasis via phagocytosis of dead cardiomyocytes.[2]

In a comparison of the 4 clusters to signatures of key immune processes and populations,[19] cluster 3 was associated with M2 polarization, matching its pro-repair identity (dark dots in Figure IVC in the online-only Data Supplement), whereas the other 3 clusters were associated with enhanced glycolytic activity, a sign of leukocyte activation (Figure IVC in the online-only Data Supplement). Indeed, clusters 4, 5, and 8 significantly expressed mRNA signals for proinflammatory cytokine IL (interleukin) 1β (Figure 2G), hallmark of a proinflammatory M1-like phenotype. The CCR2⁺ M1-like clusters (4 and 8), likely to be bone marrow–derived monocytes/macrophages, significantly expressed proinflammatory cytokine oncostatin M (Osm) (Figure 2H). Osm expression by macrophages in the heart promotes organ dysfunction.[20] Validating these findings, we found significantly higher expression of Osm mRNA through quantitative polymerase chain reaction in TAC- versus sham-operated mouse hearts at 1 week after operation, matching the known early-onset effect of macrophages in the heart[3] (Figure IVD in the online-only Data Supplement). The Osm receptor was also detectable in mouse cardiomyocytes (Figure IVE in the online-only Data Supplement). We found Osm protein expressed in heart biopsies of human patients undergoing valvular surgery, either aortic or mitral, although not in a healthy control specimen (Figure 2I, and Figure IVF in the online-only Data Supplement).

To investigate the differences between the 3 M1-like clusters, we performed differential expression analysis on clusters 4 and 8 versus cluster 5. Genes differentially expressed in clusters 4 and 8 were significantly associated with Gene Ontologies for oxidative phosphorylation and tricarboxylic acid cycle, indicative of cell activation (Figure IVG in the online-only Data Supplement). Cluster 5 showed significant association with mitogen-activated protein kinase pathway signatures, indicating that all 3 populations were undergoing activation, albeit following different transcriptional programs. Cluster 5 could be further subdivided into 2 subclusters (Figure IIC in the online-only Data Supplement), one of which (subcluster 18) differentially expressed repair-associated genes *Mmp9* and *Arg2* and neutrophil-associated gene *Csf3r* (Figure IVH in the online-only Data Supplement).

In response to disease, cluster 8 showed an increase in TAC over sham both at 1 and 4 weeks, and cluster 4 at 4 weeks (Figure 2J, Tables II and III in the online-only Data Supplement), whereas the cardiac resident clusters 3 and 5 showed a small increase at both time points. Thus, analysis of the monocyte/macrophage clusters confirms, at a single-cell level, that the heart contains resident CCR2⁻ M2-like antigen-presenting (pro-repair) macrophages (cluster 3), CCR2⁻ M1-like phagocytic monocyte/macrophages (cluster 5), and proinflammatory, M1-like CCR2⁺ Osm⁺ Il1b⁺ recruited populations (clusters 4 and 8), as well. Induction of disease results in increases in abundance of all populations, to different extents.

B Cell Subpopulations in the Heart

B cells were abundant in the heart, even in the absence of disease induction (Figures 1F and 2K, Tables II and III

Figure 1 Continued. TAC at 1 week, and purple: TAC at 4 weeks). **D**, Heat map showing the top 50 most differentially expressed genes in each cluster identified through unsupervised clustering of cardiac immune cells. Light blue indicates lower expression; dark blue indicates higher expression. Average expression (avg. exp) scale is shown on the right. Known cell type markers strongly and specifically associated with major cell types are shown on the right. **E**, Heat map representing Pearson correlations between the 20 cell populations identified through unsupervised clustering of cardiac immune cells. Pearson correlation coefficient is shown above, colored according to the degree of correlation (from light gray to dark blue). **F**, Bar plot showing the proportions of cells in each of the 20 identified cell populations, colored according to cluster designation. Identified cell types are shown on the right. FACS indicates fluorescence-activated cell sorting; MHC, major histocompatibility complex; NK, Natural Killer; Osm, oncostatin M; and scRNA-seq, single-cell RNA-sequencing; TAC, transverse aortic constriction; and Treg, regulatory T cells.

Downloaded from http://ahajournals.org by on July 24, 2023

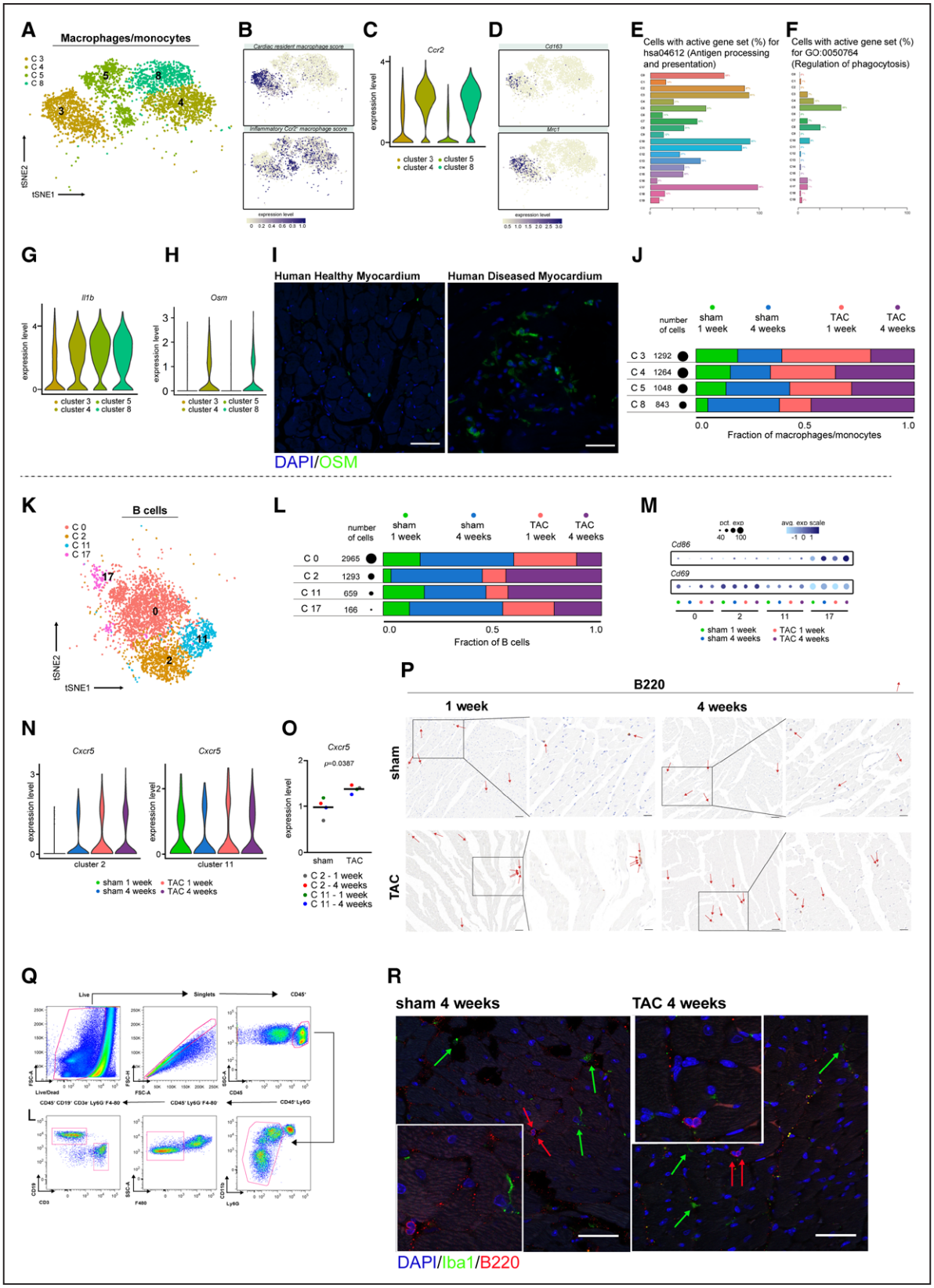

Figure 2. Cardiac macrophages/monocytes can be divided into 1 cluster of pro-repair resident, 2 clusters of CCR2⁺Osm⁺ proinflammatory, and 1 cluster of phagocytic macrophages/monocytes.

A, t-SNE projection of the 4 macrophage clusters identified in the heart of sham- and TAC-operated mice (clusters 3, 4, 5, and 8). **B**, Feature plot showing cardiac resident macrophage score and inflammatory Ccr2+ macrophage score identified within macrophage/monocyte populations. Each point depicts a single cell, colored according to normalized expression levels. Average expression scale is shown below. For each gene set, only cells expressing an expression value greater than the first quantile are shown. A complete list of genes used to compute enrichment is provided in the Expanded Methods in the online-only Data Supplement. (*Continued*)

Downloaded from http://ahajournals.org by on July 24, 2023

in the online-only Data Supplement). We identified 4 B cell populations: clusters 0, 2, 11, and 17, expressing unique B cell markers (Figure 1D and Figures III and VA in the online-only Data Supplement) and significantly enriched for B cell receptor signaling signatures (Figure VB in the online-only Data Supplement). Cluster 0 was distinct from other B cell clusters in the resolution tree (Figure IIC in the online-only Data Supplement). In response to disease, the relative abundance of cluster 0 was reduced in TAC-operated animals in comparison with sham at 4 weeks. However, cluster 2 expanded in TAC-operated animals (in comparison with sham) at both 1 and 4 weeks, whereas cluster 11, which coclusters with cluster 2 in the resolution tree (Figure IIC in the online-only Data Supplement), expanded at 4 weeks (Figure 2L and Tables II and III in the online-only Data Supplement). This suggested that clusters 2 and 11 are activated in response to cardiac stress. Activation marker *Cd86* was highly expressed in a subset of cells in clusters 2 and 11 (smaller but darker dots in Figure 2M) but was also expressed in cluster 17 (Figure 2M and Figure VC in the online-only Data Supplement). Clusters 2 and 11 significantly expressed mRNA for B cell activation marker *Cd69*[21] (Figure 2M and Figure VC in the online-only Data Supplement). Gene set variation analysis on all 4 clusters (0, 2, 11, and 17) demonstrated significant association of clusters 2 and 11 with B cell activation (Figure VD in the online-only Data Supplement). Cluster 0, least prone to activation with disease, contained 2 minor constituent subsets in the resolution tree (Figure IIC in the online-only Data Supplement), one of which differentially expressed activation-related genes (Figure VE in the online-only Data Supplement). Thus, distinctions regarding activation state, even for B cell clusters showing limited response to disease (0 and 17), most likely form a continuum and are not strictly binary.

Both B cell clusters 2 and 11 expressed significantly higher mean levels of *Cxcr5* after TAC, a chemokine receptor required for organizing B cells into follicles within lymph nodes,[22] and whose ligand suffices to generate tertiary lymph nodes[23] (Figure 2N and 2O). All B cell clusters also expressed *Ccr7* (Figure VF in the online-only Data Supplement), which can lead B cells toward lymph node T cell zones. This raised the possibility that B and T cells could be organized into tertiary lymph nodes, as they do in the atherosclerotic aortic adventitia.[24] To assess this, we examined paraffin-embedded sections of hearts from TAC- or sham-operated mice by immunohistochemistry for B cell marker B220. B cells were clearly present within the myocardium, occasionally clustered together, yet falling short of canonical follicle architecture (Figure 2P and Figure VG in the online-only Data Supplement). Because the absolute abundance of the B cells in the sections was not as marked as we would expect from the sc-Seq results, we performed flow cytometric analysis for B cell marker CD19 on TAC- or sham-operated mouse hearts; this confirmed their presence, yielding a clear signal for B cells in the heart (Figure 2Q). To further validate their presence within the myocardium and their relative abundance in comparison with macrophages/monocytes, we performed tissue clarification procedures, via the X-CLARITY system, on entire hearts, enabling the immunofluorescent staining of whole tissue with anti-B220 for B cells and anti-Iba1 for macrophages (Figure 2R and Figure VIA and VIB in the online-only Data Supplement). The images confirmed the presence of B cells (Figure 2R, red arrows) interspersed between cardiomyocytes (Figure 2R, elongated cells visible in the background) within the myocardium, occasionally in small clusters, although less abundant than macrophages (green arrows).

Figure 2 Continued. **C**, Expression distribution (violin plot) showing normalized expression levels of the *Ccr2* gene in macrophages/monocytes (clusters 3, 4, 5, and 8). **D**, Feature plot showing *Cd163* and *Mrc1* gene expression gradients identified within macrophage/monocyte populations. Each point depicts a single cell, colored according to normalized expression levels. Average expression scale is shown below. For each gene, only cells expressing an expression value greater than the first quartile are shown. **E**, Percentage of cells with active gene sets for KEGG_Antigen Processing and Presentation among all clusters. **F**, Percentage of cells with active gene sets for GO_Regulation of Phagocytosis among all clusters. **G**, Expression distribution (violin plot) showing normalized expression levels of *Il1b* gene in clusters 3, 4, 5, and 8. **H**, Expression distribution (violin plot) showing normalized expression levels of *Osm* gene in clusters 3, 4, 5, and 8. **I**, Representative images of immunofluorescent staining of Osm (green) in human ventricular biopsies of patients undergoing surgery for cardiac pathologies versus human ventricular biopsy of a healthy control (original magnification ×40; scale bar=50 µm). **J**, Bar plot showing the proportions of cells in each condition (sham at 1 week, sham at 4 weeks, TAC at 1 week, and TAC at 4 weeks) for each macrophage/monocyte cluster identified (3, 4, 5, and 8). Total number of cells identified in each cluster is shown on the left side, with dot size proportional to the number of cells in each cluster. **K**, B cells are abundantly present in the myocardium, subdivided into 4 clusters, and become activated and expand in heart failure. t-SNE projection of the 4 clusters of B cells identified in the heart of sham- and TAC-operated mice (clusters 0, 2, 11, and 17). **L**, Bar plot showing the proportions of cells in each condition (sham at 1 week, sham at 4 weeks, TAC at 1 week, and TAC at 4 weeks) for each B cell cluster identified (0, 2, 11, and 17). Total number of cells identified in each cluster is shown on the left, with dot size proportional to the number of cells in each cluster. **M**, Dot plot of *Cd86* and *Cd69* gene expression values in each of the 4 B cell clusters, and in each of the 4 groups. Dot size represents the proportion of cells expressing the gene at an expression value greater than indicated (pct. exp), whereas dot intensity (from light blue to dark blue) is proportional to the average expression (avg. exp) value of all cells expressing *Cd86* and *Cd69*, respectively. **N**, Expression distribution (violin plots) showing normalized expression levels of *Cxcr5* gene, in cluster 2 (**Left**) and in cluster 11 (**Right**), in the 4 conditions. **O**, *Cxcr5* expression in the sham group (clusters 2 and 11 at 1 week and 4 weeks) and the TAC group (clusters 2 and 11 at 1 week and 4 weeks). Bars represent grand means. To compare means, unpaired 2-tailed student *t* test was used. **P**, Representative images of immunohistochemical staining for the B cell marker B220 (brown coloration and red arrows; original magnification ×20; scale bar=50 µm) in hearts of TAC- and sham-operated mice at 1 and 4 weeks after the operation and zoomed-in images (scale bar=20µm). **Q**, Representative gating strategy for FACS analysis of B cell presence in hearts of TAC- or sham-operated mice. Live cells were gated, doublets were excluded, and $CD45^+$ cells were identified. $CD11b^+$ $F480^+$ and $CD3e^+$ cells were excluded. $CD19^+$ positive cells were identified as B cells. **R**, Representative images of immunofluorescent staining for the B cell marker B220 (red) and macrophage marker Iba1 in clarified hearts of sham- and TAC-operated C57BL6/J male mice 4 weeks after surgery (red arrows, B220 for B cells; green arrows, Iba1 for macrophages; original magnification ×40; scale bar=50 µm) and zoomed-in detail (small squares). DAPI indicates 4′,6-diamidino-2-phenylindole; FACS, fluorescence-activated cell sorting; OSM, Oncostatin M; TAC, transverse aortic constriction; and t-SNE, *t*-distributed stochastic neighbor embedding.

Downloaded from http://ahajournals.org by on July 24, 2023

In summary, B cells are present within the myocardium in health and disease. Upon induction of pressure overload, subsets of B cells become activated and expand (or are recruited from the periphery), both at the early and late stage of disease.

Activated T Cells Expand in Response to Disease

Although both CD8+ and CD4+ T cells are present in HF, the latter are considered more important for disease development.[4,25,26] We identified distinct clusters for CD8+ (clusters 6 and 15) and CD4+ T cells (clusters 9 and 13) (Figure 1D, Figure III in the online-only Data Supplement, Figure 3A, and Figure VIIA in the online-only Data Supplement). The CD4+ and CD8+ T cells were similar in relative abundance overall (Figure 3B, Tables II and III in the online-only Data Supplement), confirmed by flow cytometry (Figure VIIB in the online-only Data Supplement). Cluster 13 CD4+ T cells and cluster 15 CD8+ T cells showed a relative expansion with disease at 4 weeks after TAC (Figure 3C, Tables II and III in the online-only Data Supplement). T cells proliferate only after activation, and indeed the 2 clusters expanding with late-stage disease expressed higher levels of activation marker *Cd69* and T cell zone–associated chemokine receptor *Ccr7* (Figure 3D). To assess whether the latter enabled the formation of T cell clusters, we examined paraffin-embedded sections by immunohistochemistry for T and B cells; both T and B cells were clearly identifiable within the myocardium (brown: T cells; purple: B cells), although the occasional clusters involved mostly B cells and were of limited size (Figure 3E). These findings suggest that clusters 13 and 15 represent CD4+ and CD8+ T cells undergoing activation. However, clusters 6 and 9 shrank at the late stage of disease. T cells must be activated by antigen to migrate from lymphoid organs toward and into tissues.[27] Clusters 6 and 9 did not express markers associated with naive cells, and thus cannot be designated naive T cells; yet, because they were tissue associated, they may be antigen primed but not fully activated.

In unsupervised Reactome signature analysis, clusters 13 and 15 were significantly associated with T cell receptor signaling pathways, confirming their activated status (Figure VIIC in the online-only Data Supplement). Reactome gene ontology analysis of the differential expression (6 versus 15; 9 versus 13) showed correlation of CD8+ cluster 15 with lymphocyte activation, differentiation, and proliferation Gene Ontologies (Figure VIID in the online-only Data Supplement), and of CD4+ cluster 13 with cell activation Gene Ontology and cytokine signaling Kyoto Encyclopedia of Genes and Genomes (Figure VIIE in the online-only Data Supplement), fitting the effector functions of CD8+ and CD4+ T cells, respectively. Last, we examined the clusters against signatures of CD8+ T cells from scRNA-seq studies.[28] The activated cluster 15 was associated with stem cell memory and effector CD8+ T cell signatures (Figure 3F). In summary, antigen-experienced CD4+ and CD8+ T cell subsets are present in the myocardium, where they become further activated and expand in response to pressure overload.

Treg and Other T Cell Subsets

Cluster 14 (Figure 1D, Figure III in the online-only Data Supplement, Figure 3G, and Figure VIIIA in the online-only Data Supplement), expressed mRNA signals for key Treg markers *Foxp3*, *Tnfrsf18* (GITR), and *Ctla4* (Figure 3H), and correlated significantly with induced or natural Treg rather than conventional T cell gene set enrichment analysis signatures (Figure VIIIB in the online-only Data Supplement). The cluster was also identified as Treg in a comparison with T cell subpopulation signatures[19] and via Gene Atlas analysis (Figure VIIIC in the online-only Data Supplement). The Treg cluster did not change substantially in relative abundance between TAC- and sham-operated animals (Figure 3I, and Tables II and III in the online-only Data Supplement).

We identified a further minor, nonexpanding T cell–like subset in cluster 18 (Figures 1C, Figure III in the online-only Data Supplement, Figure 3G, and Figure VIIIA in the online-only Data Supplement). These cells expressed T cell–specific markers, such as *Thy1*, but oddly also coexpressed T-helper 17 marker gene *Rora*, T-helper 2 marker gene *Gata3*, Arginine 1 (*Arg1*), but also *Tnfrsf18* (GITR) (Figure 3H and 3J). Reactome analysis identified significant associations with signaling via IL-4 and IL-13 (Figure VIIID in the online-only Data Supplement), hallmarks of T-helper 2 cells, yet the T cell signature had a significant but not a strong association with Treg[19] (Figure VIIIC in the online-only Data Supplement). Gene set enrichment analysis signature analysis yielded a higher correlation with T-helper 17 cells than with Treg (Figure VIIID in the online-only Data Supplement), raising the possibility that the cluster is an unstable Treg population.[29] Yet because the levels of T cell marker *Cd3e* in cluster 18 were lower than those of all other T cell subsets (Figure VIIIE in the online-only Data Supplement), we cannot exclude possible similarity to an ILC2 population previously identified in healthy mouse hearts.[8] Studies at even higher resolution will be required to ascertain the exact identity of this population.

Gene *Pdcd1* encodes T cell exhaustion marker PD-1. It is found in activated T cells, and its inhibitory effects on T cell function are detrimental when T cell activity is required, eg, in antitumor responses. PD-1 also promotes the immunosuppressive function of Treg/induced Tregs.[30,31] Of the 118 cells that were expressing *Pdcd1* in the samples we analyzed, 78% mapped to clusters 14 and 18 (Figure VIIIF and VIIIG in the online-only Data Supplement), with greater enrichment in TAC-operated hearts over sham (Fisher test P=0.02) (Figure 3K, top); this was more evident at 1 week after TAC, as confirmed

Downloaded from http://ahajournals.org by on July 24, 2023

Figure 3. Heart failure induces the expansion of both CD4⁺- and CD8⁺-activated T cells.

A, t-SNE projection of 4 clusters of T cells identified in the heart of sham- and TAC-operated mice (clusters 6, 9, 13, and 15). **B**, Bar plot showing the proportions of cells in each condition (sham at 1 week, sham at 4 weeks, TAC at 1 week, and TAC at 4 weeks) for CD8⁺ T cells (clusters 6 and 15) and for CD4⁺ T cells (clusters 9 and 13). Total number of cells identified for each cell type is shown on the left, with dot size proportional to the number of cells in each subgroup. **C**, Bar plot showing the proportions of cells in each condition (sham at 1 week, sham at 4 weeks, TAC at 1 week, and TAC at 4 weeks) for each T cell cluster identified (6, 9, 13, and 15). Total number of cells identified in each cluster is shown on the left, with dot size proportional to the number of cells in each cluster. (*Continued*)

Downloaded from http://ahajournals.org by on July 24, 2023

by flow cytometry (Figure 3K, middle and lower) and quantitative polymerase chain reaction (Figure VIIIH in the online-only Data Supplement). Because immunosuppressive cells will oppose cardiotoxic inflammation, inhibition of immunosuppressive function should boost cardiotoxicity. Indeed, mice treated with blocking anti–PD-1 antibody, a tumor therapy anti-immunosuppressive agent, developed significant cardiac T cell expansion (judged by lineage marker *Cd3e*), M1-polarized inflammation (judged by cardiac expression of type 1 cytokines IL-1β, interferon-γ, and tumor necrosis factor-α) (Figure 3L), and reduction in heart functionality (Figure 3M).

Neutrophils

Neutrophils are the first immune cells recruited to a site of inflammation. We detected 2 distinct neutrophil clusters, clusters 7 and 16 (Figure 1D, Figure III in the online-only Data Supplement, Figure 4A, and Figure IXA in the online-only Data Supplement). Both significantly expressed neutrophil marker *Csf3r* (Figure IXA in the online-only Data Supplement and Figure 4B), and both expanded at 4 weeks after TAC (Figure 4C, and Tables II and III in the online-only Data Supplement). Both were significantly associated with neutrophil degranulation via Reactome analysis (Figure IXB in the online-only Data Supplement), yet the 2 clusters had clear differences. Cluster 7 significantly expressed much higher mRNA signals for chemokine receptor CCR2, usually expressed on inflammatory monocytes and neutrophils.[32] However, cluster 16 featured higher expression of mRNA for CXCR2 and CCR1 (Figure IXC in the online-only Data Supplement). This was confirmed by flow cytometry, because CCR2$^+$ cardiac-infiltrating neutrophils had significantly lower levels of CXCR2 surface expression, whereas CCR2$^-$ neutrophils expressed more CXCR2 (Figure IXD in the online-only Data Supplement). Differential expression analysis highlighted significantly higher expression of activation marker *Cd69*[33] in cluster 7, as opposed to pro-repair genes[34] *Mmp9* and *Arg2* in cluster 16 (Figure IXE in the online-only Data Supplement). Unsupervised gene signature analysis on the differentially expressed genes revealed significant correlation of cluster 7 but not 16 with transcriptional activity and antigen presentation (Figure IXF in the online-only Data Supplement). Thus, clusters 7 and 16 may represent a larger proinflammatory and a smaller pro-repair neutrophil subset, respectively, which respond in parallel to pressure overload. Their differential chemokine receptor expression may also signify distinct microenvironment localization patterns.

NK Cells

A small population of cardiac NK cells has been previously identified, without further insight.[8] We identified 2 distinct NK cell clusters (1 and 12) (Figure 4D), by their expression of NK-specific markers (Figure 1D, and Figures III and XA in the online-only Data Supplement), by Mouse Gene Atlas analysis (Figure 4E), and by analysis against NK-specific signatures (Figure XB in the online-only Data Supplement). The only notable change in relative abundance with disease was the expansion of the smaller cluster, cluster 12, at 1 week after TAC (Figure 4F). Both clusters significantly expressed mRNA for proinflammatory cytokine interferon-γ (Figure 4G), yet differential expression analysis of cluster 1 versus 12 identified significant enrichment of activation marker *Cd69* and significant association with immune activation and cytokine production pathways (Figure XC and XD in the online-only Data Supplement) in cluster 12, suggesting that the smaller, expanding NK population is most likely undergoing activation with the onset of disease.

Figure 3 Continued. **D**, Dot plot of *Cd69* and *Ccr7* gene expression value in T cell clusters (6, 9, 13, and 15). Dot size represents the proportion of cells expressing the gene at an expression value greater than indicated (pct. exp), whereas dot intensity (from light blue to dark blue) is proportional to the average expression (avg. exp) value of all cells expressing *Cd69* and *Ccr7*, respectively. **E**, Representative images of double immunohistochemical staining for the B cell marker B220 (red coloration and red arrows) and T cell marker CD3 (brown coloration and brown arrows) in hearts of TAC- and sham-operated mice at 1 and 4 weeks after the operation (original magnification ×20; scale bar=50 μm). **F**, Dot plot of CD8$^+$ effector score and stem cell–like memory score in CD8$^+$ T cells (clusters 6 and 15). Dot size represents the proportion of cells expressing the gene set at an expression value greater than indicated (pct. exp), whereas dot intensity (from light blue to dark blue) is proportional to the average expression value of the gene set score. A complete list of genes used to compute enrichment is provided in the Expanded Methods in the online-only data supplement. **G**, PD-1$^+$ regulatory T cells and T cell–like cells in the heart. t-SNE projection of Treg and T cell–like clusters (clusters 14 and 18) in the heart of sham- and TAC-operated mice. **H**, Dot plot of *Foxp3*, *Tnfrsf18*, and *Ctla4* gene expression values in all clusters. Dot size represents the proportion of cells expressing the gene at an expression value greater than indicated (pct. exp), whereas dot intensity (from light blue to dark blue) is proportional to the average expression value of all cells expressing *Foxp3*, *Tnfrsf18*, and *Ctla4*, respectively. Cluster 14 is highlighted. **I**, Bar plot showing the proportions of cells in each condition (sham at 1 week, sham at 4 weeks, TAC at 1 week, and TAC at 4 weeks) for each cluster identified (14 and 18). Total number of cells identified in each cluster is shown on the left, with dot size proportional to the number of cells in each cluster. **J**, Dot plot of *Thy1*, *Rora*, *Gata3*, and *Arg1* gene expression values in all clusters. Dot size represents the proportion of cells expressing the gene at an expression value greater than indicated (pct. exp), whereas dot intensity (from light blue to dark blue) is proportional to the average expression value of all cells expressing *Thy1*, *Rora*, *Gata3*, and *Arg1*, respectively. Cluster 18 is highlighted. **K**, **Top**, Expression distribution (violin plot) showing normalized expression levels of *Pdcd1* gene in clusters 14 and 18 *Pdcd1*$^+$ cells. **Middle**, FACS analysis of PD1$^+$ Treg in heart of TAC- and sham-operated mice. Percentage of PD1$^+$ cells out of Foxp3$^+$ CD4$^+$ CD45$^+$ live cells, isolated from hearts of TAC- and sham-operated mice, 1 and 4 weeks after surgery, are plotted as mean±SEM, each dot represents one mouse (n=3-5; *P<0.05; 1-way ANOVA, Tukey post test). **Bottom**, Representative concatenated FACS plot of PD1$^+$ cells (green for sham 1 week, blue for sham 4 weeks, red for TAC 1 week, and purple for TAC 4 weeks) gated on Foxp3$^+$ CD4$^+$ CD45$^+$ live cells (gray dots). Each dot represents one cell. **L**, Relative mRNA expression of *Cd3e, Il6, Ifng*, and *Tnfa* in hearts of C57BL6/J male mice after 2 weeks of antitumor therapy with blocking anti–PD-1 antibody or IgG isotype control. Each dot represents one mouse (n=8+8). Data plotted as means±SEM (*P<0.05; **P<0.01; ***P<0.001; Mann-Whitney test). **M**, Ejection fraction (%EF) and fractional shortening (%FS) analyzed via echocardiography of C57BL6/J male mice injected for 2 weeks with neutralizing anti–PD-1 antibody or IgG isotype control. Each dot represents one mouse (n=3). Data plotted as means±SEM (*P<0.05). Unpaired *t* test. FACS indicates fluorescence-activated cell sorting; IgG, immunoglobulin G; TAC, transverse aortic constriction; Treg, regulatory T cells; and t-SNE, *t*-distributed stochastic neighbor embedding.

Downloaded from http://ahajournals.org by on July 24, 2023

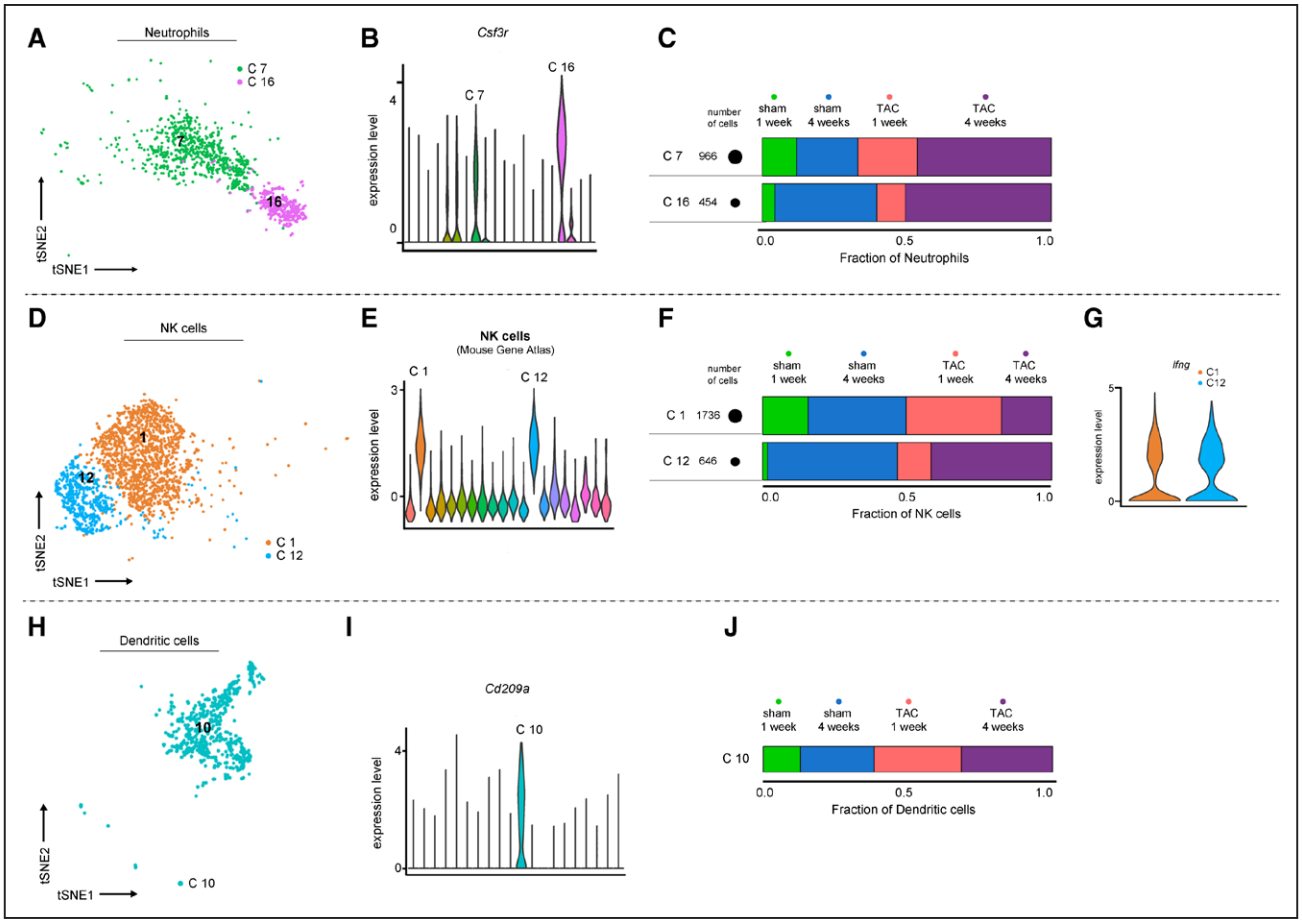

Figure 4. Heart failure–related inflammation recruits 2 distinct neutrophil subsets into the heart.
A, t-SNE projection of neutrophil clusters identified (clusters 7 and 16) in the heart of sham- and TAC-operated mice. **B**, Expression distribution (violin plot) showing normalized expression levels of *Csf3r* gene in neutrophil cells (clusters 7 and 16). Clusters 7 and 16 are labeled. **C**, Bar plot showing the proportions of cells in each condition (sham at 1 week, sham at 4 weeks, TAC at 1 week, and TAC at 4 weeks) for each T cell cluster identified (7 and 16). Total number of cells identified in each cluster is shown on the left, with dot size proportional to the number of cells in each cluster. **D**, Cardiac NK cells activate and expand after TAC. t-SNE projection of NK cell clusters identified (clusters 1 and 12) in the heart of sham- and TAC-operated mice. **E**, Expression distribution (violin plot) showing normalized expression levels of NK cell gene signatures in all identified clusters. Clusters 1 and 12 are highlighted. Complete list of genes used to compute enrichment are provided in the Expanded Methods in the online-only Data Supplement. **F**, Bar plot showing the proportions of cells in each condition (sham at 1 week, sham at 4 weeks, TAC at 1 week, and TAC at 4 weeks) for each NK cell cluster identified (1 and 12). Total number of cells identified in each cluster is shown on the left, with dot size proportional to the number of cells in each cluster. **G**, Expression distribution (violin plot) showing normalized expression levels of *Ifng* gene in clusters 1 and 12. **H**, CD209⁺ dendritic cells are present in the heart. t-SNE projection of the dendritic cell cluster identified (cluster 10) in the heart of sham- and TAC-operated mice. **I**, Expression distribution (violin plot) showing normalized expression levels of *Cd209a* gene in all clusters. Cluster 10 is highlighted. **J**, Bar plot showing the proportions of cells in each condition (sham at 1 week, sham at 4 weeks, TAC at 1 week, and TAC at 4 weeks) in cluster 10. NK indicates Natural Killer; TAC, transverse aortic constriction; and t-SNE, *t*-distributed stochastic neighbor embedding.

Dendritic Cells

Dendritic cells (DCs) were identified in cluster 10, expressing MHC II (H2) molecules and DC marker DC-SIGN (*Cd209a*) (Figure 4H, Figures III and XIA in the online-only Data Supplement, and Figure 4I). Their relative abundance was decreased with diseased state, both at 1 and 4 weeks after TAC (Figure 4J, Tables II and III in the online-only Data Supplement). Unsupervised analysis via Mouse Gene Atlas identified the cluster as myeloid DCs (Figure XIB in the online-only Data Supplement). Cluster 10 was not homogeneous but could be subdivided into 2 subclusters (Figure IIC in the online-only Data Supplement). Reactome analysis of the differentially expressed genes between the subclusters identified the larger subset as more transcriptionally active and associated with DC differentiation (Figure XIC in the online-only Data Supplement).

Mast Cells

A role for mast cells in heart disease was proposed >2 decades ago.[15] scRNA-seq studies have not detected them, possibly for lack of sufficient resolution. Cluster 19 (Figures 1B and 5A) expressed mast cell marker *Mcpt8* (Figure 5B and 5C, and Figure III in the online-only Data Supplement), and the mast cell– and type 2–associated cytokines IL-4 and IL-13 (Figure 5D). Mouse Gene Atlas analysis confirmed a significant association with mast cell signature (Figure XID in the online-only Data Supplement). Although this was the least abundant cluster

Downloaded from http://ahajournals.org by on July 24, 2023

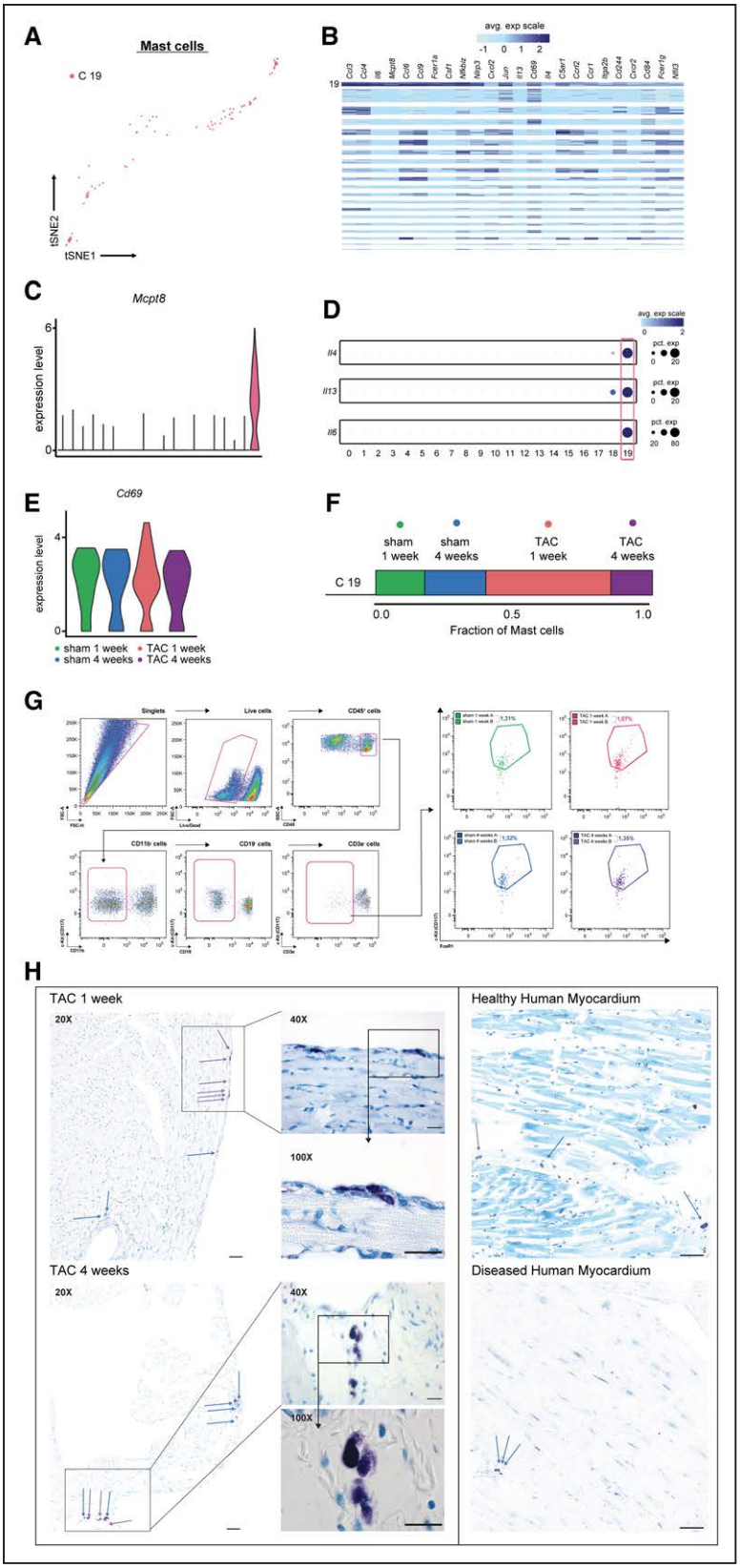

Figure 5. Mast cells are present in the myocardium and epicardium and highly upregulate expression of proinflammatory cytokine interleukin 6.
A, t-SNE projection of the mast cell cluster identified (cluster 19) in the heart of sham- and TAC-operated mice. **B**, Heat map showing the average expression (avg. exp) value of 24 mast cell marker genes. We defined a gene to be a cluster-specific marker if it was differentially upregulated in a specific cluster, in comparison with each of the remaining clusters. Average expression scale is shown above. **C**, Expression distribution (violin plot) showing normalized expression levels of *Mcpt8* gene in all clusters. **D**, Dot plot of *Il4*, *Il13*, and *Il6* gene expression values in all clusters. Dot size represents the proportion of cells expressing the gene at an expression value greater than indicated (pct. exp), whereas dot intensity (from light blue to dark blue) is proportional to the average expression value of all cells expressing *Il4*, *Il13*, and *Il6*, respectively. Cluster 19 is highlighted. **E**, Expression distribution (violin plot) showing normalized expression levels of *Cd69* gene in cluster 19. **F**, Bar plot showing the proportions of cells in each condition (sham at 1 week, sham at 4 weeks, TAC at 1 week, and TAC at 4 weeks) in mast cell cluster 19. **G**, Representative gating strategy for FACS analysis of mast cell presence in hearts of TAC- or sham-operated mice. Live cells were gated, doublets were excluded, and CD45$^+$ cells were identified. CD11b$^-$ CD19$^-$ CD3e$^-$ cells were excluded. c-Kit (CD117) and FceR1 double-positive cells were identified as mast cells. The 4 plots on the right report the mean percentage of mast cells out of CD45$^+$ cells from 2 replicates for each condition (green: sham 1 week; red: TAC 1 week; blue: sham 4 weeks; purple: TAC 4 weeks). **H**, **Left**, Representative images of mast cell staining with toluidine blue of hearts of TAC- and sham-operated mice at 1 and 4 weeks after the operation. Purple arrows indicate degranulating mast cells and blue arrows indicate nondegranulating mast cells (original magnification ×20, ×40, and ×100; scale bar=50 μm; the representative sections shown are from TAC 1- and 4-week time points). **Right**, Representative images of mast cell staining with toluidine blue of human ventricular biopsies of healthy control and human ventricular biopsies of patients with cardiac pathologies. Purple arrows indicate degranulating mast cells and blue arrows indicate nondegranulating mast cells (original magnification ×20; scale bar=100 μm). FACS indicates fluorescence-activated cell sorting; TAC, transverse aortic constriction; and t-SNE, *t*-distributed stochastic neighbor embedding.

(Figure 1F), its cells upregulated mRNA for activation marker CD69 at 1 week after TAC (Figure 5E), indicative of involvement in the early response to disease. Mast cells had the highest expression of proinflammatory cytokine *Il6* (Figure 5D). IL-6 drives the cardiotoxic inflammation underlying HF.[35] Thus, a possible noncardiomyocyte source of IL-6 could be mast cells. Flow cytometry analysis confirmed mast cell presence in both healthy

Downloaded from http://ahajournals.org by on July 24, 2023

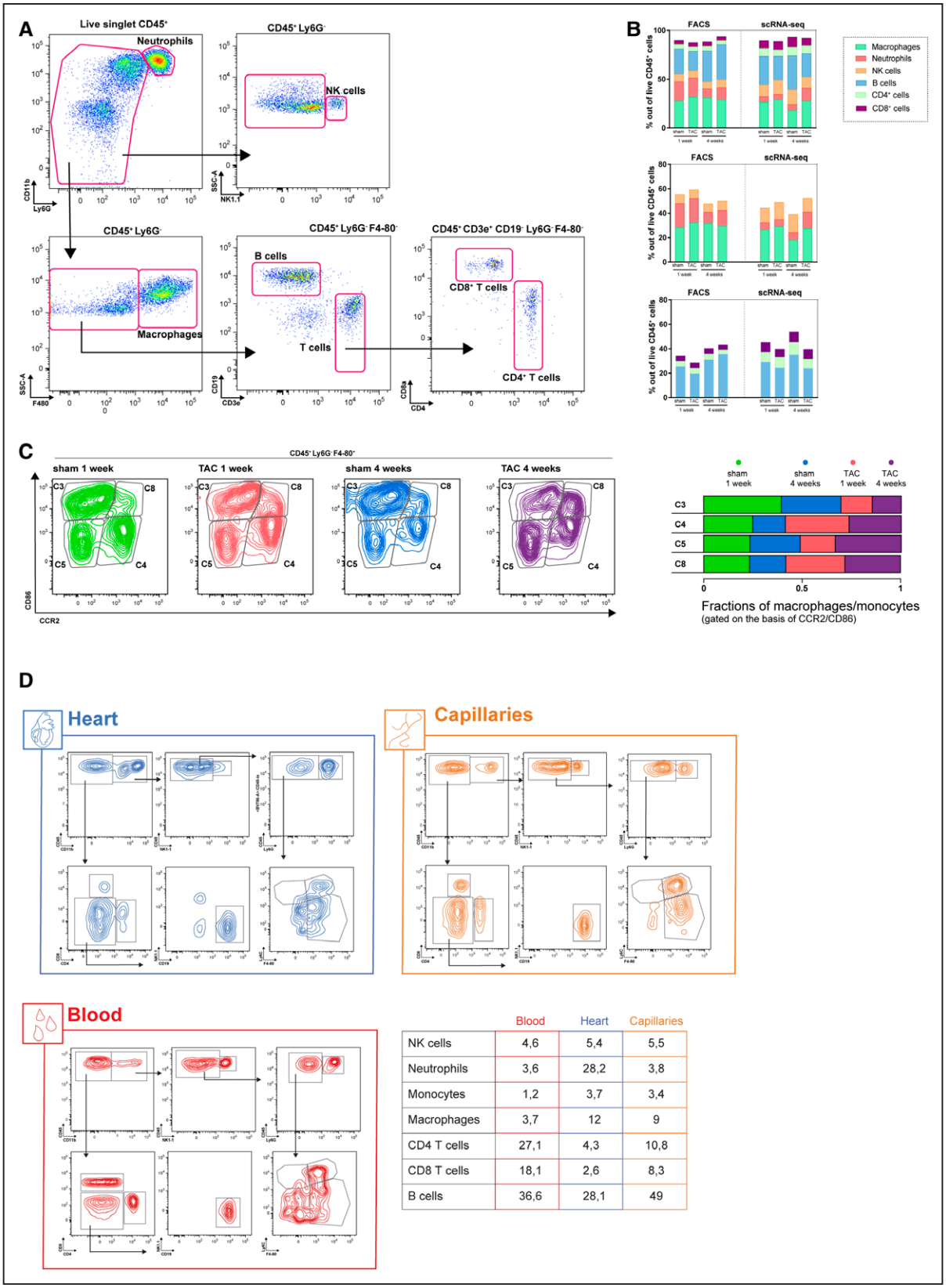

	Blood	Heart	Capillaries
NK cells	4,6	5,4	5,5
Neutrophils	3,6	28,2	3,8
Monocytes	1,2	3,7	3,4
Macrophages	3,7	12	9
CD4 T cells	27,1	4,3	10,8
CD8 T cells	18,1	2,6	8,3
B cells	36,6	28,1	49

Figure 6. FACS validation of the main immune cell populations identified via scRNA-seq confirms the expression of lineage markers in the heart. **A**, Representative gating strategy for FACS analysis used to identify the immune populations in hearts of TAC- or sham-operated mice. **B**, Bar graphs showing the percentage of immune cell populations from the hearts of TAC- or sham-operated mice, at 1 and 4 weeks after operation, identified by FACS analysis (4 bars on the left) or with scRNA-seq analysis (4 bars on the right). The abundance of each subset is plotted as the percentage of each population out of CD45+ cells, identified as in **A**. The top graph shows macrophages, neutrophils, NK cells, B cells, CD4+ and CD8+ T cells (n=7). The middle graph shows macrophages, neutrophils, and NK cells (n=7). The bottom graph shows B cells, CD4+ and CD8+ T cells (n=5). **C**, Macrophage subsets, identified as above, (*Continued*)

Downloaded from http://ahajournals.org by on July 24, 2023

and diseased hearts (Figure 5G). To investigate their exact localization in the heart, we performed toluidine blue stains (Figure 5H), revealing, in all conditions, clusters of nondegranulating (blue arrows) and degranulating (purple arrows) mast cells. Unlike all other immune subsets, mast cells appeared both within the myocardium and in the epicardium, at the periphery of the heart. Mast cells were also present in human heart biopsy sections from healthy or cardiopathic subjects (Figure 5H).

Validation

scRNA-seq identifies clusters from a large number of genes contributing to the cluster-defining identity, with superior precision in comparison with methods on the basis of a single or few parameters, such as flow cytometry and microscopy. We did, nonetheless, use different techniques to validate scRNA-seq findings (Figure 2I, 2P through 2R, 3E and 3K, 5G and 5H and Figures IVD through IVF, VG, VI, VIIB, VIIIH, and IXC in the online-only Data Supplement). With the exception of very low frequency subsets, cell subsets were identifiable by multiparameter flow cytometry by using the gating shown (Figure 6A). Relative abundance ratios of subsets identified through flow cytometry versus scRNA-seq (Figure 6B, top) were similar but not identical. This could be because of the limitations of lineage definition by a limited set of markers. Closer inspection of innate and adaptive ratios (Figure 6B, middle and bottom) shows the largest difference originating from increased representation of neutrophils in flow cytometry. Reduced RNA yields from neutrophils could affect the number of neutrophils detectable via scRNA-seq. Yet, it is unlikely to affect the qualitative features of the 2 subpopulations we identified by Gene Ontology analysis. For the more abundant cell populations, it was possible to closely replicate the scRNA-seq findings. Surface expression of CCR2 and CD86 on F4-80$^+$ macrophage cells from sham- or TAC-operated hearts (Figure 6C) revealed 4 distinct subpopulations, matching the scRNA-seq clustering (Figure 2), as did surface expression of CCR2 and MHC II (Figure XIE in the online-only Data Supplement).

As mentioned earlier (Figure IIA in the online-only Data Supplement), staining with anti-CD45 before cell isolation[13] allowed assessment of the extent of cells found in cardiac capillaries rather than within the heart itself, which would be analyzed as cardiac-infiltrating cells in most studies. For most immune subsets, relative abundance in the capillaries closely mirrored their distribution in the heart rather than in peripheral blood (Figure 6D), signifying that immune cells present in the capillaries are not likely to be a contamination of circulating peripheral blood cells. Interesting exceptions were neutrophils, enriched in the heart but scarce in the capillaries and peripheral blood, and B cells, highly abundant in all 3 compartments, but mostly in capillaries. This may reflect active migration patterns and will merit further study.

Global Differences Between TAC and Sham

Differential expression analysis of the 2 TAC-operated time points versus their sham-operated counterparts, independently of clusters, highlighted significant upregulation of proinflammatory cytokine *Il1b*, chemokine receptor *Ccr2*, and monocyte/macrophage markers *Cd14*/*Cd68* (Figure 7A), reflecting the activation and recruitment of M1-like monocyte/macrophage populations. At 1 week, there was significant differential upregulation of MHC class II molecules, implicating antigen presentation by macrophages, B cells, or DCs.

Gene set variation analysis across the 4 different states highlights variations at a larger scale. Differentially enriched gene signatures in the diseased state included B cell activation, MHC class I signaling/cross-presentation (the latter signs of CD8$^+$ T cell involvement). Also evident were signatures related to DNA synthesis, mitosis, and cell replication, indicative of proliferating immune cells, a result of activation (Figure 7B). These features recapitulate the findings of the cluster-based analysis, that monocyte/macrophages, T cells, and B cells are activated by the induction of disease. A few signatures were found to be significantly enriched only at the 1- or 4-week TAC-operated time point, respectively. At 1 week, these were related to adaptive immunity, compatible with our identification of B cell activation at early time points. At the 4-week time point, anti-inflammatory pathway signatures for transforming growth factor β and CTLA4 (cytotoxic T-lymphocyte–associated protein 4) were enriched (Figure 7B through 7D). *Ctla4* gene expression was maximal at 4 weeks after TAC, mostly on cluster 14, the Treg.

Figure 6 Continued. were further gated as CCR2$^-$ CD86$^+$ (cluster 3), CCR2$^-$ CD86$^-$ (cluster 5), CCR2$^+$ CD86$^+$ (cluster 8), and CCR2$^+$ CD86$^-$ (cluster 4). Each contour plot is representative of one condition (green: sham 1 week; red: TAC 1 week; blue: sham 4 weeks; purple: TAC 4 weeks). Bar plot showing the proportions of each macrophage/monocyte population in each condition (green: sham 1 week; red: TAC 1 week; blue: sham 4 weeks; purple: TAC 4 weeks). **D**, C57BL6/J male mice were injected intravenously with anti-CD45-PECy7 and euthanized 1 minute after injection. Hearts were washed or perfused with PBS, blood from the chamber was collected in EDTA. Single-cell suspensions from heart and blood were analyzed via flow cytometry for lineage markers, including CD45 via anti-CD45-BV786. CD45$^+$ cells marked with anti-CD45-PECy7 were considered leukocytes from capillaries. CD45$^+$ cells collected from the heart with no signal for CD45-PECy7, marked only with anti-CD45-BV786, were considered true heart-infiltrating cells. Representative gating strategy for FACS analysis used to identify the immune populations from hearts (blue), capillaries (orange), and peripheral blood (red). Table shows the percentage out of live CD45$^+$ cells for the leukocyte populations. FACS indicates fluorescence-activated cell sorting; NK, Natural Killer; scRNA-seq, single-cell RNA-sequencing; and TAC, transverse aortic constriction.

Downloaded from http://ahajournals.org by on July 24, 2023

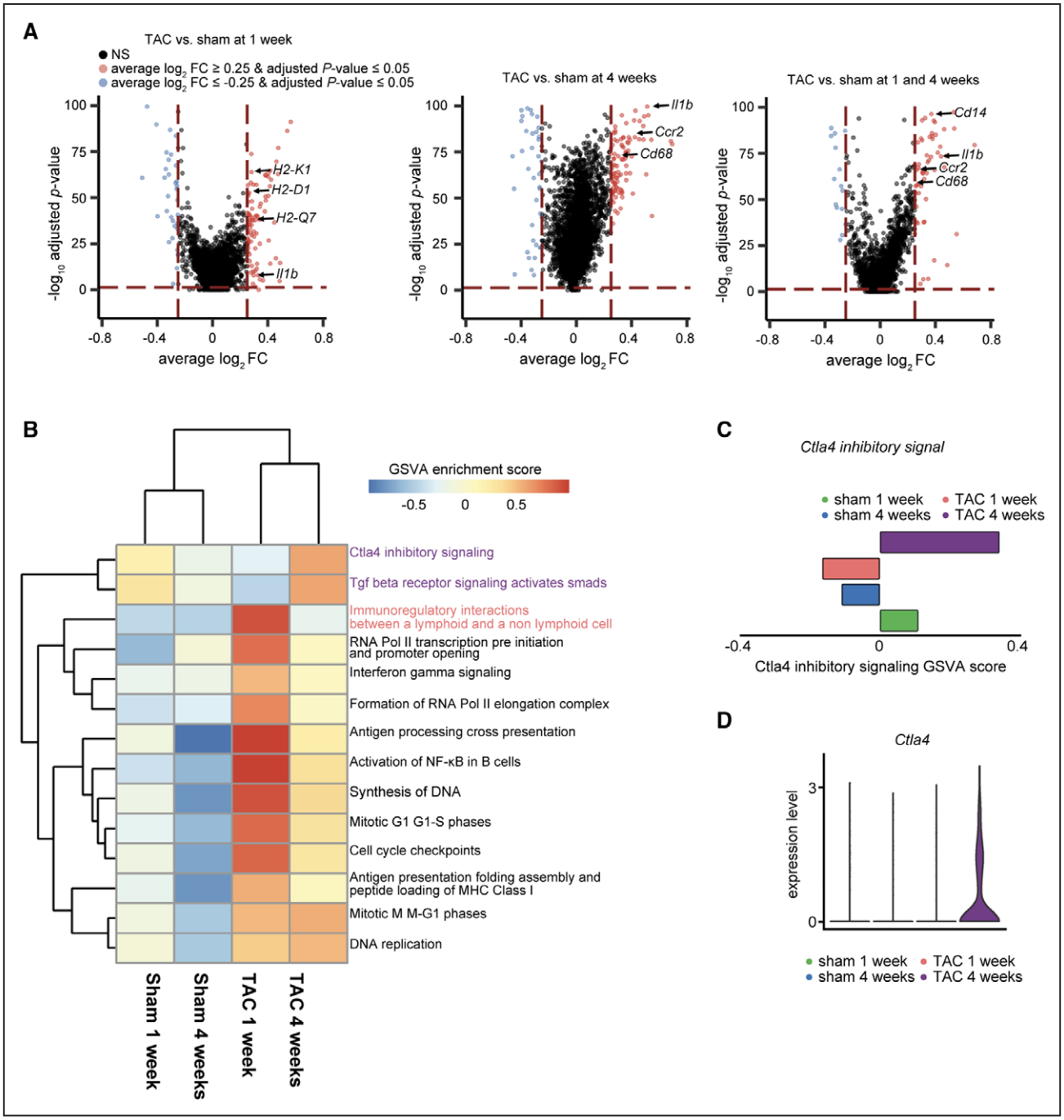

Figure 7. Cluster-independent differences between TAC- and sham-operated mice confirm cluster analysis findings.
A, Volcano plots of the differentially modulated genes in TAC versus sham at 1 week (**Left**), TAC versus sham at 4 weeks (**Middle**), and in all TAC versus all sham (**Right**). The *x* axis specifies the average $\log_2$ fold changes (FC) and the *y* axis specifies the negative logarithm (base 10) of the adjusted *P* values. Red vertical and horizontal lines reflect the filtering criteria (average $\log_2$ FC=±0.25 and adjusted *P*=0.05). Red dots indicate genes whose expression is induced in TAC, blue dots indicate genes whose expression is reduced in TAC. Representative genes are labeled. **B**, Heat map showing top enriched terms assessed through GSVA. GSVA enrichment score is shown above. Highlighted in violet are processes enriched in the TAC 4-week group, whereas highlighted in red are enriched in the TAC 1-week group. Highlighted in black are processes enriched at both TAC 1- and 4-week groups. Euclidean distance was used to calculate row and column clustering. **C**, Representative enriched process (Ctla4 inhibitory signaling) is shown through a bar plot. **D**, Expression distribution (violin plot) showing normalized expression levels of the *Ctla4* gene in all clusters. GSVA indicates gene set variation analysis; and TAC, transverse aortic constriction.

DISCUSSION

We analyzed, using scRNA-seq, the immune subpopulations present in the hearts of mice with pressure overload, at early and late time points. The results show, remarkably, a wide range of innate and adaptive immune cells responding to pressure overload by becoming activated and expanding (Figure 8). This happens in the myocardium, and the epicardium in the case of mast cells. This would not be surprising in viral or

Downloaded from http://ahajournals.org by on July 24, 2023

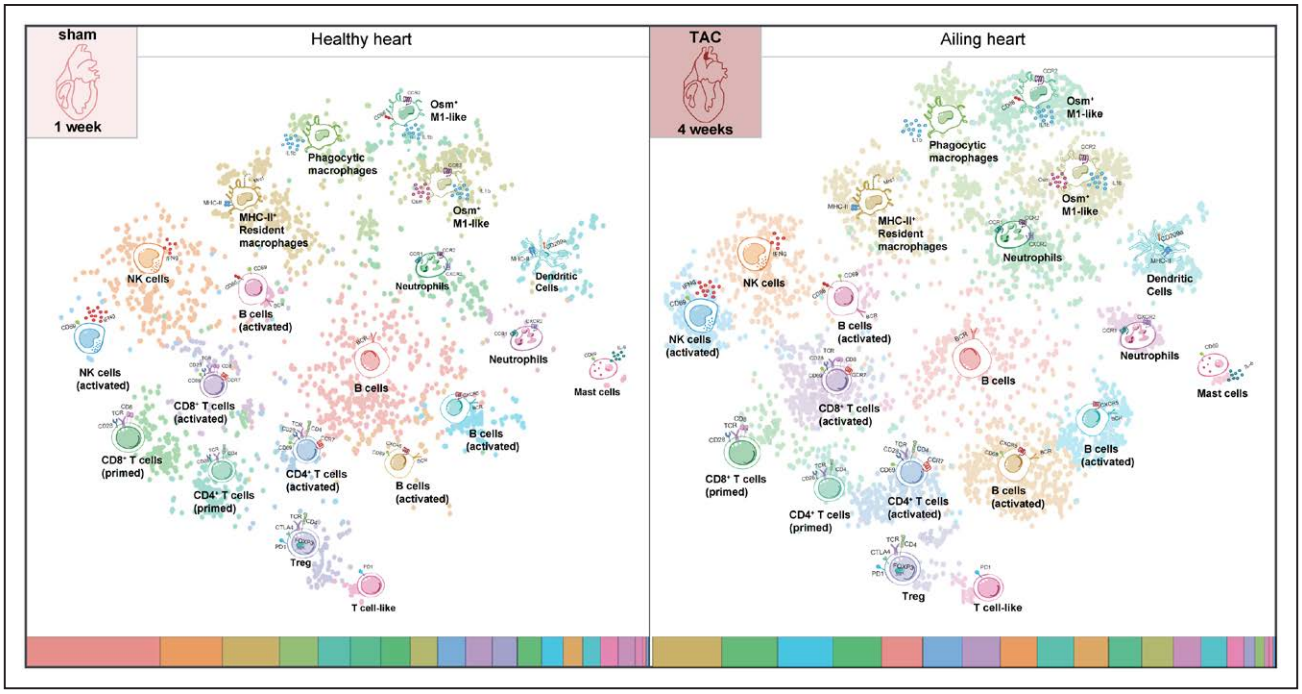

Figure 8. Graphical summary of the immune cell subsets identified in the heart of sham- or TAC-operated mice.
Labels correspond to cluster identities and relevant selected marker genes. MHC indicates major histocompatibility complex; NK, Natural Killer; Osm, oncostatin M; TAC, transverse aortic constriction; and Treg, regulatory T cells.

autoimmune myocarditis.[36] We describe a similarly complete immune response occurring as a result of hemodynamic stress. Stressed cardiomyocytes produce proinflammatory cytokines, such as IL-6.[37] Immune cells amplify cytokine signaling; we identified mast cells, often found at the start of immune responses, to be present in the epicardium and myocardium and strong producers of *Il6*. This rekindles decades-old hypotheses on the involvement of mast cells in HF.[15,16]

Macrophages and T cells are required for the progression of cardiac disease.[3–6] After decades of autoimmunity studies, substantial knowledge exists on how they function in close coordination with all other immune subsets. This includes neutrophils and NK cells, which responded to disease, the latter possibly in a protective role.[38] In type 2–polarized conditions, eosinophils could also appear.[39] The presence of nonhomogeneous DC populations must be considered in light of their distinct roles in myocarditis[40] and the response to myocardial infarction.[41] Our high-resolution mapping of these subpopulations can now enable the accumulated immunological insight to be applied to the study of HF.

Monocyte/macrophage subpopulations clustered into cardiac resident versus recruited proinflammatory subsets, with distinct functions.[2,3,17] The resident clusters (3 and 5) did show a small expansion with disease, as previously reported.[3] Our finding that the proinflammatory cytokine-producing, M1 clusters 4 and 8, and cardiac patient hearts, as well, express cytokine Osm is intriguing; Osm production was recently shown to mediate refractivity from anti–tumor necrosis factor therapies in inflammatory bowel disease.[42] This may offer a novel explanation for the failure of anti–tumor necrosis factor therapy trials in patients with HF.[36] The expression of Osm receptor in cardiomyocytes is compatible with a direct effect of Osm on cardiomyocytes.[20]

Few studies have examined the role of B cells in HF.[43–45] Activated B cell clusters 2 and 11 expressed high levels of *Cd86*. CD86 is an activator of T cell costimulation and a target for inhibitor molecule CTLA4. Pharmacological administration of CTLA4-Ig, a US Food and Drug Administration–approved, CTLA4-based drug, has therapeutic effects on the TAC model of HF.[6] The expression of the CTLA4 target, CD86, on activated B cells explains why the CTLA4-mediated effect is dependent on the presence of B cells.[6]

T cells expanded and expressed more activation markers with disease, although clusters 6 and 9 did not expand. Yet, because they were de facto tissue-homing T cells, they must be antigen primed.[46] Expression of CXCR5 in B cells and CCR7 in T cells could potentially guide them into follicles and T cell zones, respectively. Apart from limited B cell clustering, we did not find tertiary lymph node–like accumulations. This transcriptional activity may be a feature of B cell and T cell activation, evolved to deal with infectious agents and not sterile cardiac inflammation. Other mechanisms may also be guiding T cells in the heart, as previously shown.[47]

Immunosuppressive Tregs inhibit cardiotoxic inflammation if their numbers are augmented experimentally.[48] In the context of pathological inflammation, Tregs increase their numbers without effect, in an insufficient

Downloaded from http://ahajournals.org by on July 24, 2023

attempt at suppression, as shown in atherosclerosis.[49] In pressure overload, they expand significantly only at a very advanced stage (8 weeks after TAC).[6] Consistently, we found that numbers of Tregs were stable at 1 and 4 weeks of disease; they were nonetheless active, showing PD-1(*Pdcd1*) expression at 1 week and *Ctla4* at 4 weeks. The expression of PD-1 offers an explanation for recent reports of anti–PD-1 treatment in cancer immunotherapy leading to fatal myocarditis.[50] Indeed, we found significantly increased T cell presence, inflammation, and reduced functionality in hearts of anti–PD-1–treated mice.

The standard control for the TAC model is a sham operation, where the thread is passed by the aorta but not ligated. We have shown[6] that this does induce limited inflammation, albeit significantly less than TAC. Most notable differences related to sham occurred in activated NK cells (cluster 12), which expanded in 4 weeks after sham. However, the abundance of the cluster was greater in the TAC than the sham at each individual time point.

Our analysis delineates how the immune cells in the myocardium and epicardium become activated and expand on the induction of pressure overload, mirroring classical immune responses, even though no pathogen or autoimmune trigger is present. We identified, at high resolution, the characteristics of the subsets of immune cell types involved in this response, and the molecules conducting this activation signal; these are included in the generated data set. Detailed investigation of these markers and molecules may offer new diagnostic or therapeutic targets of clinical relevance for HF.

ARTICLE INFORMATION

Received May 13, 2019; accepted November 4, 2019.

The online-only Data Supplement is available with this article at https://www.ahajournals.org/doi/suppl/10.1161/CIRCULATIONAHA.119.041694.

Authors

Elisa Martini, PhD*; Paolo Kunderfranco, PhD*; Clelia Peano, PhD; Pierluigi Carullo, PhD; Marco Cremonesi, MSc; Tilo Schorn, PhD; Roberta Carriero, PhD; Alberto Termanini, PhD; Federico Simone Colombo, PhD; Elena Jachetti, PhD; Cristina Panico, MD; Giuseppe Faggian, MD; Andrea Fumero, MD; Lucia Torracca, MD; Martina Molgora, PhD; Javier Cibella, MSc; Christina Pagiatakis, PhD; Jolanda Brummelman, PhD; Giorgia Alvisi, MSc; Emilia Maria Cristina Mazza, PhD; Mario Paolo Colombo, PhD; Enrico Lugli, PhD; Gianluigi Condorelli, MD, PhD; Marinos Kallikourdis, PhD

Correspondence

Gianluigi Condorelli, MD, PhD, Via Manzoni 56, Rozzano 20089, Italy; or Marinos Kallikourdis, PhD, Via Manzoni 56, Rozzano 20089, Italy. Email gianluigi.condorelli@humanitasresearch.it or marinos.kallikourdis@humanitasresearch.it

Affiliations

Adaptive Immunity Laboratory (E.M., M.C., M.K.), Bioinformatics Unit (P.K., R.C., A.T.), Genomic Unit (C. Peano, J.C.), Department of Cardiovascular Medicine (P.C., C. Panico, C. Pagiatakis, G.C.), Advanced Imaging Unit (T.S.), Flow Cytometry Core (F.S.C., E.L.), Cardiac Surgery Division, Department of Cardiovascular Medicine (A.F., L.T.), Laboratory of Experimental Immunopathology (M.M.), Laboratory of Translational Immunology (J.B., G.A., E.M.C., E.L.), Humanitas Clinical and Research Center, Rozzano, Milan, Italy. Institute of Genetic and Biomedical Research, UoS Milan, National Research Council, Rozzano, Italy (C. Peano, P.C., G.C.). Molecular Immunology Unit, Department of Research, Fondazione IRCCS Istituto Nazionale dei Tumori, Milan, Italy (E.J., M.P.C.). Department of Cardiac Surgery, University of Verona, Italy (G.F.). Humanitas University, Pieve Emanuele, Italy (G.C., M.K.).

Acknowledgments

Dr Martini performed isolation of cells, coordinated overall experimental process and scheduling, guided the data analysis at detailed level, performed multiparameter flow cytometry and immunohistochemistry, produced figures, wrote methods and figure legends; Dr Kunderfranco performed all bioinformatics analysis, produced figures, wrote methods and figure legends; Dr Peano was involved in experimental design, performed and supervised single-cell sequencing experiments and wrote methods; Dr Carullo performed TAC and sham surgery; Dr Cremonesi assisted with isolation of cells for sequencing and with flow cytometry experiments; Dr Schorn performed the clarification analysis, Drs Carriero and Termanini assisted with bioinformatic analysis; Dr F.S. Colombo performed cell sorting, contributed to design of sorting protocol; Dr Jachetti performed the mast cell staining; Dr Panico contributed to discussions of results; Drs Faggian, Fumero, and Torracca provided human biopsies; Dr Molgora provided the anti-PD-1–treated mouse hearts; Dr Cibella performed sequencing; Dr Pagiatakis provided cardiomyocytes; Drs Brummelman and Alvisi advised on the multiparameter flow cytometry analysis; Dr Mazza performed bioinformatic analysis of multiparameter flow cytometry; Dr M.P. Colombo supervised the mast cell analysis; Dr Lugli supervised the multiparameter flow cytometry analysis; Dr Condorelli ideated the project, interpreted results, and provided adequate resources for the experiments; and Dr Kallikourdis supervised the project, guided the data analysis, and wrote the article.

Sources of Funding

This work was supported by Ministry of Health, Cardiovascular Network Project "Plaque," European Research Council (ERC) Advanced Grant (CardioEpigen, No. 294609), and Fondazione Regionale per la Ricerca Biomedica CP2_14/2018 (to Dr Condorelli) and Cariplo grant 2014-1184 (to Dr Kallikourdis).

Disclosures

None.

REFERENCES

1. Shioi T, Matsumori A, Kihara Y, Inoko M, Ono K, Iwanaga Y, Yamada T, Iwasaki A, Matsushima K, Sasayama S. Increased expression of interleukin-1 beta and monocyte chemotactic and activating factor/monocyte chemoattractant protein-1 in the hypertrophied and failing heart with pressure overload. *Circ Res.* 1997;81:664–671. doi: 10.1161/01.res.81.5.664
2. Epelman S, Lavine KJ, Beaudin AE, Sojka DK, Carrero JA, Calderon B, Brija T, Gautier EL, Ivanov S, Satpathy AT,et al. Embryonic and adult-derived resident cardiac macrophages are maintained through distinct mechanisms at steady state and during inflammation. *Immunity.* 2014;40:91–104. doi: 10.1016/j.immuni.2013.11.019
3. Patel B, Bansal SS, Ismahil MA, Hamid T, Rokosh G, Mack M, Prabhu SD. CCR2+ monocyte-derived infiltrating macrophages are required for adverse cardiac remodeling during pressure overload. *JACC Basic Transl Sci.* 2018;3:230–244. doi: 10.1016/j.jacbts.2017.12.006
4. Laroumanie F, Douin-Echinard V, Pozzo J, Lairez O, Tortosa F, Vinel C, Delage C, Calise D, Dutaur M, Parini A, et al. CD4+ T cells promote the transition from hypertrophy to heart failure during chronic pressure overload. *Circulation.* 2014;129:2111–2124. doi: 10.1161/CIRCULATIONAHA.113.007101
5. Nevers T, Salvador AM, Grodecki-Pena A, Knapp A, Velázquez F, Aronovitz M, Kapur NK, Karas RH, Blanton RM, Alcaide P. Left ventricular T-Cell recruitment contributes to the pathogenesis of heart failure. *Circ Heart Fail.* 2015;8:776–787. doi: 10.1161/CIRCHEARTFAILURE.115.002225
6. Kallikourdis M, Martini E, Carullo P, Sardi C, Roselli G, Greco CM, Vignali D, Riva F, Ormbostad Berre AM, Stølen TO, et al. T cell costimulation blockade blunts pressure overload-induced heart failure. *Nat Commun.* 2017;8:14680. doi: 10.1038/ncomms14680
7. Ridker PM, Everett BM, Thuren T, MacFadyen JG, Chang WH, Ballantyne C, Fonseca F, Nicolau J, Koenig W, Anker SD, et al; CANTOS Trial Group. Antiinflammatory therapy with canakinumab for atherosclerotic disease. *N Engl J Med.* 2017;377:1119–1131. doi: 10.1056/NEJMoa1707914

Downloaded from http://ahajournals.org by on July 24, 2023

8. Skelly DA, Squiers GT, McLellan MA, Bolisetty MT, Robson P, Rosenthal NA, Pinto AR. Single-cell transcriptional profiling reveals cellular diversity and intercommunication in the mouse heart. *Cell Rep.* 2018;22:600–610. doi: 10.1016/j.celrep.2017.12.072
9. The Tabula Muris Consortium, Overall Coordination, Logistical Coordination, Organ Collection and Processing, Library Preparation and sequencing, Computational data analysis, Cell type annotation, Writing group, Supplemental text writing group, Principal Investigators. Single-cell transcriptomics of 20 mouse organs creates a Tabula Muris. *Nature*. 2018;562:367-372. doi: 10.1038/s41586-018-0590-4
10. Gladka MM, Molenaar B, de Ruiter H, van der Elst S, Tsui H, Versteeg D, Lacraz GPA, Huibers MMH, van Oudenaarden A, van Rooij E. Single-cell sequencing of the healthy and diseased heart reveals cytoskeleton-associated protein 4 as a new modulator of fibroblasts activation. *Circulation.* 2018;138:166–180. doi: 10.1161/CIRCULATIONAHA.117.030742
11. Rockman HA, Ross RS, Harris AN, Knowlton KU, Steinhelper ME, Field LJ, Ross J Jr, Chien KR. Segregation of atrial-specific and inducible expression of an atrial natriuretic factor transgene in an *in vivo* murine model of cardiac hypertrophy. *Proc Natl Acad Sci USA.* 1991;88:8277–8281. doi: 10.1073/pnas.88.18.8277
12. Dirkx E, Gladka MM, Philippen LE, Armand AS, Kinet V, Leptidis S, El Azzouzi H, Salic K, Bourajjaj M, da Silva GJ, et al. Nfat and miR-25 cooperate to reactivate the transcription factor Hand2 in heart failure. *Nat Cell Biol.* 2013;15:1282–1293. doi: 10.1038/ncb2866
13. Bansal SS, Ismahil MA, Goel M, Zhou G, Rokosh G, Hamid T, Prabhu SD. Dysfunctional and proinflammatory regulatory T-lymphocytes are essential for adverse cardiac remodeling in ischemic cardiomyopathy. *Circulation.* 2019;139:206–221. doi: 10.1161/CIRCULATIONAHA.118.036065
14. Butler A, Hoffman P, Smibert P, Papalexi E, Satija R. Integrating single-cell transcriptomic data across different conditions, technologies, and species. *Nat Biotechnol.* 2018;36:411–420. doi: 10.1038/nbt.4096
15. Patella V, Marinò I, Arbustini E, Lamparter-Schummert B, Verga L, Adt M, Marone G. Stem cell factor in mast cells and increased mast cell density in idiopathic and ischemic cardiomyopathy. *Circulation.* 1998;97:971–978. doi: 10.1161/01.cir.97.10.971
16. Hara M, Matsumori A, Ono K, Kido H, Hwang MW, Miyamoto T, Iwasaki A, Okada M, Nakatani K, Sasayama S. Mast cells cause apoptosis of cardiomyocytes and proliferation of other intramyocardial cells *in vitro*. *Circulation.* 1999;100:1443–1449. doi: 10.1161/01.cir.100.13.1443
17. Bajpai G, Schneider C, Wong N, Bredemeyer A, Hulsmans M, Nahrendorf M, Epelman S, Kreisel D, Liu Y, Itoh A, et al. The human heart contains distinct macrophage subsets with divergent origins and functions. *Nat Med.* 2018;24:1234–1245. doi: 10.1038/s41591-018-0059-x
18. Dick SA, Macklin JA, Nejat S, Momen A, Clemente-Casares X, Althagafi MG, Chen J, Kantores C, Hosseinzadeh S, Aronoff L, et al. Self-renewing resident cardiac macrophages limit adverse remodeling following myocardial infarction. *Nat Immunol.* 2019;20:29–39. doi: 10.1038/s41590-018-0272-2
19. Azizi E, Carr AJ, Plitas G, Cornish AE, Konopacki C, Prabhakaran S, Nainys J, Wu K, Kiseliovas V, Setty M, et al. Single-cell map of diverse immune phenotypes in the breast tumor microenvironment. *Cell.* 2018;174:1293–1308.e36. doi: 10.1016/j.cell.2018.05.060
20. Kubin T, Pöling J, Kostin S, Gajawada P, Hein S, Rees W, Wietelmann A, Tanaka M, Lörchner H, Schimanski S, et al. Oncostatin M is a major mediator of cardiomyocyte dedifferentiation and remodeling. *Cell Stem Cell.* 2011;9:420–432. doi: 10.1016/j.stem.2011.08.013
21. Roselli G, Martini E, Lougaris V, Badolato R, Viola A, Kallikourdis M. CXCL12 mediates aberrant costimulation of b lymphocytes in warts, hypogammaglobulinemia, infections, myelokathexis immunodeficiency. *Front Immunol.* 2017;8:1068. doi: 10.3389/fimmu.2017.01068
22. Reif K, Ekland EH, Ohl L, Nakano H, Lipp M, Förster R, Cyster JG. Balanced responsiveness to chemoattractants from adjacent zones determines B-cell position. *Nature.* 2002;416:94–99. doi: 10.1038/416094a
23. Luther SA, Lopez T, Bai W, Hanahan D, Cyster JG. BLC expression in pancreatic islets causes B cell recruitment and lymphotoxin-dependent lymphoid neogenesis. *Immunity.* 2000;12:471–481. doi: 10.1016/s1074-7613(00)80199-5
24. Gräbner R, Lötzer K, Döpping S, Hildner M, Radke D, Beer M, Spanbroek R, Lippert B, Reardon CA, Getz GS, et al. Lymphotoxin beta receptor signaling promotes tertiary lymphoid organogenesis in the aorta adventitia of aged ApoE-/- mice. *J Exp Med.* 2009;206:233–248. doi: 10.1084/jem.20080752
25. Gröschel C, Sasse A, Monecke S, Röhrborn C, Elsner L, Didié M, Reupke V, Bunt G, Lichtman AH, Toischer K, et al. CD8+-T cells with specificity for a model antigen in cardiomyocytes can become activated after transverse aortic constriction but do not accelerate progression to heart failure. *Front Immunol.* 2018;9:2665. doi: 10.3389/fimmu.2018.02665
26. Ramos GC, van den Berg A, Nunes-Silva V, Weirather J, Peters L, Burkard M, Friedrich M, Pinnecker J, Abeßer M, Heinze KG, et al. Myocardial aging as a T-cell-mediated phenomenon. *Proc Natl Acad Sci U S A.* 2017;114:E2420–E2429. doi: 10.1073/pnas.1621047114
27. Vignali D, Kallikourdis M. Improving homing in T cell therapy. *Cytokine Growth Factor Rev.* 2017;36:107–116. doi: 10.1016/j.cytogfr.2017.06.009
28. Pace L, Goudot C, Zueva E, Gueguen P, Burgdorf N, Waterfall JJ, Quivy JP, Almouzni G, Amigorena S. The epigenetic control of stemness in CD8+ T cell fate commitment. *Science.* 2018;359:177–186. doi: 10.1126/science.aah6499
29. Sawant DV, Vignali DA. Once a Treg, always a Treg? *Immunol Rev.* 2014;259:173–191. doi: 10.1111/imr.12173
30. Wafula PO, Teles A, Schumacher A, Pohl K, Yagita H, Volk HD, Zenclussen AC. PD-1 but not CTLA-4 blockage abrogates the protective effect of regulatory T cells in a pregnancy murine model. *Am J Reprod Immunol.* 2009;62:283–292. doi: 10.1111/j.1600-0897.2009.00737.x
31. Francisco LM, Salinas VH, Brown KE, Vanguri VK, Freeman GJ, Kuchroo VK, Sharpe AH. PD-L1 regulates the development, maintenance, and function of induced regulatory T cells. *J Exp Med.* 2009;206:3015–3029. doi: 10.1084/jem.20090847
32. Massara M, Bonavita O, Savino B, Caronni N, Mollica Poeta V, Sironi M, Setten E, Recordati C, Crisafulli L, Ficara F, et al. ACKR2 in hematopoietic precursors as a checkpoint of neutrophil release and anti-metastatic activity. *Nat Commun.* 2018;9:676. doi: 10.1038/s41467-018-03080-8
33. Atzeni F, Schena M, Ongari AM, Carrabba M, Bonara P, Minonzio F, Capsoni F. Induction of CD69 activation molecule on human neutrophils by GM-CSF, IFN-gamma, and IFN-alpha. *Cell Immunol.* 2002;220:20–29. doi: 10.1016/s0008-8749(03)00002-9
34. Bonavita E, Gentile S, Rubino M, Maina V, Papait R, Kunderfranco P, Greco C, Feruglio F, Molgora M, Laface I, et al. PTX3 is an extrinsic oncosuppressor regulating complement-dependent inflammation in cancer. *Cell.* 2015;160:700–714. doi: 10.1016/j.cell.2015.01.004
35. Meléndez GC, McLarty JL, Levick SP, Du Y, Janicki JS, Brower GL. Interleukin 6 mediates myocardial fibrosis, concentric hypertrophy, and diastolic dysfunction in rats. *Hypertension.* 2010;56:225–231. doi: 10.1161/HYPERTENSIONAHA.109.148635
36. Mann DL. Innate immunity and the failing heart: the cytokine hypothesis revisited. *Circ Res.* 2015;116:1254–1268. doi: 10.1161/CIRCRESAHA.116.302317
37. Ancey C, Corbi P, Froger J, Delwail A, Wijdenes J, Gascan H, Potreau D, Lecron JC. Secretion of IL-6, IL-11 and LIF by human cardiomyocytes in primary culture. *Cytokine.* 2002;18:199–205. doi: 10.1006/cyto.2002.1033
38. Ong S, Rose NR, Čiháková D. Natural killer cells in inflammatory heart disease. *Clin Immunol.* 2017;175:26–33. doi: 10.1016/j.clim.2016.11.010
39. Diny NL, Baldeviano GC, Talor MV, Barin JG, Ong S, Bedja D, Hays AG, Gilotra NA, Coppens I, Rose NR, et al. Eosinophil-derived IL-4 drives progression of myocarditis to inflammatory dilated cardiomyopathy. *J Exp Med.* 2017;214:943–957. doi: 10.1084/jem.20161702
40. Van der Borght K, Scott CL, Martens L, Sichien D, Van Isterdael G, Nindl V, Saeys Y, Boon L, Ludewig B, Gillebert TC, et al. Myocarditis elicits dendritic cell and monocyte infiltration in the heart and self-antigen presentation by conventional type 2 dendritic cells. *Front Immunol.* 2018;9:2714. doi: 10.3389/fimmu.2018.02714
41. Choo EH, Lee JH, Park EH, Park HE, Jung NC, Kim TH, Koh YS, Kim E, Seung KB, Park C, et al. Infarcted myocardium-primed dendritic cells improve remodeling and cardiac function after myocardial infarction by modulating the regulatory T cell and macrophage polarization. *Circulation.* 2017;135:1444–1457. doi: 10.1161/CIRCULATIONAHA.116.023106
42. West NR, Hegazy AN, Owens BMJ, Bullers SJ, Linggi B, Buonocore S, Coccia M, Görtz D, This S, Stockenhuber K, et al; Oxford IBD Cohort Investigators. Oncostatin M drives intestinal inflammation and predicts response to tumor necrosis factor-neutralizing therapy in patients with inflammatory bowel disease. *Nat Med.* 2017;23:579–589. doi: 10.1038/nm.4307
43. Zouggari Y, Ait-Oufella H, Bonnin P, Simon T, Sage AP, Guérin C, Vilar J, Caligiuri G, Tsiantoulas D, Laurans L, et al. B lymphocytes trigger monocyte mobilization and impair heart function after acute myocardial infarction. *Nat Med.* 2013;19:1273–1280. doi: 10.1038/nm.3284
44. Keppner L, Heinrichs M, Rieckmann M, Demengeot J, Frantz S, Hofmann U, Ramos G. Antibodies aggravate the development of ischemic heart failure. *Am J Physiol Heart Circ Physiol.* 2018;315:H1358–H1367. doi: 10.1152/ajpheart.00144.2018

Downloaded from http://ahajournals.org by on July 24, 2023

45. Cordero-Reyes AM, Youker KA, Trevino AR, Celis R, Hamilton DJ, Flores-Arredondo JH, Orrego CM, Bhimaraj A, Estep JD, Torre-Amione G. Full expression of cardiomyopathy is partly dependent on B-cells: a pathway that involves cytokine activation, immunoglobulin deposition, and activation of apoptosis. *J Am Heart Assoc*. 2016; 5:e002484. doi: 10.1161/JAHA.115.002484
46. Fu H, Ward EJ, Marelli-Berg FM. Mechanisms of T cell organotropism. *Cell Mol Life Sci.* 2016;73:3009–3033. doi: 10.1007/s00018-016-2211-4
47. Komarowska I, Coe D, Wang G, Haas R, Mauro C, Kishore M, Cooper D, Nadkarni S, Fu H, Steinbruchel DA, et al. Hepatocyte growth factor receptor c-met instructs T cell cardiotropism and promotes T cell migration to the heart via autocrine chemokine release. *Immunity.* 2015;42:1087–1099. doi: 10.1016/j.immuni.2015.05.014
48. Weirather J, Hofmann UD, Beyersdorf N, Ramos GC, Vogel B, Frey A, Ertl G, Kerkau T, Frantz S. Foxp3+ CD4+ T cells improve healing after myocardial infarction by modulating monocyte/macrophage differentiation. *Circ Res.* 2014;115:55–67. doi: 10.1161/CIRCRESAHA.115.303895
49. Garetto S, Trovato AE, Lleo A, Sala F, Martini E, Betz AG, Norata GD, Invernizzi P, Kallikourdis M. Peak inflammation in atherosclerosis, primary biliary cirrhosis and autoimmune arthritis is counter-intuitively associated with regulatory T cell enrichment. *Immunobiology.* 2015;220:1025–1029. doi: 10.1016/j.imbio.2015.02.006
50. Johnson DB, Balko JM, Compton ML, Chalkias S, Gorham J, Xu Y, Hicks M, Puzanov I, Alexander MR, Bloomer TL, et al. Fulminant myocarditis with combination immune checkpoint blockade. *N Engl J Med.* 2016;375:1749–1755. doi: 10.1056/NEJMoa1609214

Downloaded from http://ahajournals.org by on July 24, 2023